

# Internal tide driven tracer transport across the continental slope

Carl P. Spingys<sup>1,2</sup>, Richard G. Williams<sup>1</sup>, Joanne E. Hopkins<sup>3</sup>, Rob A. Hall<sup>4</sup>,  
J. A. Mattias Green<sup>5</sup>, and Jonathan Sharples<sup>1,3</sup>

<sup>1</sup>Department of Earth, Ocean and Ecological Sciences, School of Environmental Science, University of Liverpool, UK

<sup>2</sup>Ocean and Earth Science, National Oceanography Centre, University of Southampton, Southampton, UK

<sup>3</sup>National Oceanography Centre, Liverpool, UK

<sup>4</sup>Centre for Ocean and Atmospheric Sciences, School of Environmental Sciences, University of East Anglia, UK

<sup>5</sup>School of Ocean Sciences, Bangor University, UK

## Key Points:

- The internal tide drives a Stokes' transport with a 3 layer reversing structure
- This Stokes' transport is observed in multiple near shelf edge moorings
- The Stokes' transport provides a supply of nutrients from the open ocean onto the shelf

---

Corresponding author: Carl P. Spingys, [c.p.spingys@soton.ac.uk](mailto:c.p.spingys@soton.ac.uk)

## Abstract

The role of the internal tide in driving tracer transport across the continental slope is examined using simplified layered theory, channel model experiments and observational diagnostics of near shelf-edge moorings. The effect of the internal tide is interpreted in terms of its Stokes' drift, which is separated into two distinct components: a bolus component, driven by the co-variance of layer thickness and the velocity; and a shear component, driven by the velocity following the movement of an interface. For a three layer ocean, in the model experiments and observations, the onshore propagation of an internal tide drives a Stokes' transport directed onshore in the surface and the bottom layers, and directed offshore in the pycnocline. This reversing structure is due to the bolus component dominating near the boundaries, while the shear component dominates at the pycnocline. In the observational diagnostics, the Stokes' transport is not cancelled by the Eulerian transport, which is mainly directed along bathymetric contours. The Stokes' drift of the internal tide then provides a systematic on shelf tracer transport if there is a tracer sink on the shelf, carried in the surface or bottom layers. Conversely, the tracer transport is directed offshore if there is a tracer source on the shelf with plumes of shelf tracer expected to be carried offshore along the pycnocline. This tracer transport as a result of the internal tide is diagnosed for heat, salt and nitrate. The depth-integrated nitrate flux is directed onto the shelf supplying nutrients to the productive shelf seas.

## Plain Language Summary

The global ocean can be split into two parts: deep open oceans, and shallow shelf seas, which are separated by the continental slope. The shelf seas have high biological productivity compared to the open ocean. This productivity requires a supply of nutrients from the open ocean, but how this happens is unknown. The continental slope limits many of the physical processes that drive nutrient transports within the global ocean. Here we evaluate, for the first time, a new process, which is not limited by the slope, for the transport of nutrients from the open ocean onto the shelf. This process is the transport of water, within certain layers, driven by waves within the ocean. These waves are generated by tides over the continental slope around much of the globe. We have observed this process in three time series taken near the continental slopes of Europe and New Zealand. These observations show a transport of water that is consistent with the wave induced process and a resultant nutrient transport onto the shelf. The nutrient transport seen is similar to observations of the size of the supply to the biology, potentially answering the question of sustaining shelf sea productivity.

## 1 Introduction

The continental slope dynamically constrains the fluid exchange between the shelf seas and open ocean [Brink, 2016]. This exchange of heat, freshwater, nutrients, trace metals and carbon is climatically important, affecting the imprint of the open ocean on the shelf seas, as well as the communication of the shelf seas with the open ocean.

The difficulty in exchanging fluid across the continental slope arises from the Taylor-Proudman theorem stating that geostrophic currents preferentially run along topographic contours for a steady flow and weak stratification. The emergence of slope currents running along bathymetric contours [Huthnance, 1984; Huthnance *et al.*, 2009] is as a consequence of the Taylor-Proudman theorem. However, fluid exchange across the continental slope is suggested by water-mass and nutrient signals extending across topographic contours; for example, anomalously salty lenses intrude onto the shelf [Lentz, 2003], suggesting tracer transport extending over 100 km [Hopkins *et al.*, 2012]. This implied fluid exchange across topographic contours then relies on the Taylor-Proudman constraint being alleviated, such as by the effects of friction, time dependence and ageostrophic motions [Brink, 1988; Simpson and McCandliss, 2012]. The surface wind stress or bottom

67 drag may drive an Ekman transport across the continental slope. For the European shelf,  
 68 the wind stress typically provides an on-shelf Ekman transport, while the bottom drag  
 69 from the interaction of the northward slope current and sea floor provides an off-shelf  
 70 transport [*Simpson and McCandliss*, 2012; *Huthnance et al.*, 2009; *Painter et al.*, 2016].  
 71 Time-dependent instability of the currents involving eddy transfers from the open ocean  
 72 to the shelf may be significant [*Stewart and Thompson*, 2015], as well as instabilities of  
 73 the slope current [*Hill*, 1995]. Observations of non-linear internal waves have also shown  
 74 a net volume transport from the open ocean onto the shelf seas [*Inall et al.*, 2001; *Zhang*  
 75 *et al.*, 2015].

76 The full Lagrangian transport within the ocean can be considered as the combi-  
 77 nation of a Eulerian transport and a Stokes' transport. In the presence of wave motions  
 78 the Stokes' transport can be substantial and should be evaluated to give the full Lagrangian  
 79 transport. Internal tides propagating onto the shelf and driving Stokes' transport pro-  
 80 vide an additional possible mechanism to break the geostrophic constraint and drive tracer  
 81 exchange across the continental slope. Tracer transport via internal tides may therefore  
 82 be particularly important for the exchange of nutrients and trace metals across the con-  
 83 tinental slope. The higher levels of biological productivity on the shelf lead to a forma-  
 84 tion of organic matter, requiring a supply of inorganic nutrients. The inorganic nutri-  
 85 ents are thought to ultimately originate from relatively nutrient-rich waters in the open  
 86 ocean [*Liu et al.*, 2010], but this exchange needs to be achieved by transport processes  
 87 avoiding the Taylor-Proudman constraint. Conversely, trace metals often have higher con-  
 88 centrations on the shelf than in the open ocean, as a result of riverine inputs and sed-  
 89 iment interactions, if these trace metals are transported from the shelf to the open ocean  
 90 they may be important in sustaining open ocean productivity.

91 In this study, we examine whether the internal tide drives a systematic volume and  
 92 tracer transport across the continental slope. In order to understand the fully nonlin-  
 93 ear volume and tracer transport associated with an internal tide, the Stokes' transport  
 94 is defined over a density layer [*McDougall and McIntosh*, 2001] (Section 2). The Stokes'  
 95 transport is illustrated for an internal tide using an idealised two-dimensional model sim-  
 96 ulation in a channel with and without rotation (Section 3). The transport across the con-  
 97 tinental slope is diagnosed for three different moorings located near the shelf edge and  
 98 interpreted in terms of the Stokes' transport and its contributions (Section 4). The ef-  
 99 fect of the Stokes' transport in providing a tracer transport across the continental slope  
 100 is discussed and evaluated for heat, salt and nutrients for one of the moorings (Section 5).  
 101 Finally, the potential role of the Stokes' transport in driving the exchange of other trac-  
 102 ers in the context of other processes is discussed (Section 6).

## 103 2 The Stokes' transport associated with an internal tide

104 The Stokes' transport is now considered for an internal tide. Internal tides are gen-  
 105 erated by cross-slope barotropic tidal flows interacting with stratification. Over the con-  
 106 tinental shelf and slope, the internal wave field is typically dominated by internal tide  
 107 energy [*MacKinnon and Gregg*, 2003] and at any given location the observed internal  
 108 tide may have both locally and remotely generated components [*Kelly and Nash*, 2010;  
 109 *Nash et al.*, 2012]. Part of the internal tidal energy propagates over the continental slope  
 110 and onto the shelf seas, where much of that energy is ultimately dissipated. For exam-  
 111 ple, the low-mode internal tide may propagate from the continental slope onto the shelf  
 112 and remain coherent for scales of tens to hundreds of kilometers [*Green et al.*, 2008; *In-*  
 113 *all et al.*, 2011; *Nash et al.*, 2012].

114 Internal waves can drive a non-zero Stokes' drift over some depth ranges [*Thorpe*,  
 115 1968; *Wunsch*, 1971; *Weber and Brostrom*, 2014; *Henderson*, 2016]. Recent theoretical  
 116 and numerical work demonstrated the potential for internal wave driven Stokes' drift to  
 117 transport both neutrally-buoyant and depth-regulating phytoplankton across the shelf

118 [Franks *et al.*, 2019]. However, if there is no significant mixing, the Stokes' drift from in-  
 119 ternal waves is expected to be balanced by an opposing Eulerian velocity if there is a slop-  
 120 ing bottom connected to a land boundary [Wunsch, 1971; Ou and Maas, 1986]. For an  
 121 inviscid ocean with rotation, Stokes' drift driven by an internal wave is found to be can-  
 122 celled by the Eulerian flow without invoking a closed domain [Wagner and Young, 2015],  
 123 although this cancellation may not hold for an unsteady wave [Thomas *et al.*, 2018]. This  
 124 local cancellation of the Stokes' drift from internal waves by the Eulerian flow is found  
 125 to occur in a realistic numerical model of the Antarctic slope [Stewart *et al.*, 2019] and  
 126 partially occur on a sloping lake bed [Henderson, 2016]. However, the net cancellation  
 127 may not always occur if there is strong diapycnal mixing or temporal evolution of the  
 128 current.

129 A net transport within an individual density layer may occur due to strong diapy-  
 130 cnal mixing driving volume exchange between density layers. This diapycnal mixing on  
 131 the shelf may be associated with the tides or surface winds, and may peak either with  
 132 the spring-neap cycle or the passage of atmospheric storms respectively. There is also  
 133 the possibility that temporal changes in the forcing lead to a temporal adjustment of the  
 134 currents and Stokes' drift, which may not exactly cancel if there is insufficient time for  
 135 the isopycnal slope and Eulerian transport to respond.

136 Through this paper we will explore to what extent the cancellation between the  
 137 Stokes' transport and Eulerian transport holds in idealised numerical modelling and ob-  
 138 servations.

## 139 2.1 Volume transport for a density layer

140 Following *McDougall and McIntosh* [2001], consider the fully nonlinear, volume trans-  
 141 port for a density layer,  $U(t)$ , per unit horizontal distance (in  $\text{m}^2\text{s}^{-1}$ ) between two bound-  
 142 ing density surfaces,  $\eta_1(t)$  and  $\eta_2(t)$ ,

$$U(t) = \int_{\eta_1(t)}^{\eta_2(t)} \mathbf{u}(z, t) dz = \langle \mathbf{u}(t) \rangle h(t), \quad (1)$$

143 where the layer thickness,  $h(t) = \eta_2(t) - \eta_1(t)$ ,  $\mathbf{u}(z, t)$  is the velocity vector and  $z$  is  
 144 the vertical co-ordinate, the brackets  $\langle \rangle$  denote a layer average between the bounding sur-  
 145 faces, such that the layer-average velocity is given by  $\langle \mathbf{u} \rangle = \int_{\eta_1}^{\eta_2} \mathbf{u} dz / (\eta_2 - \eta_1)$ . The  
 146 total volume transport within the layer may be separated into an Eulerian and a Stokes'  
 147 component,

$$U(t) = U_e(t) + U_s(t), \quad (2)$$

148 where the Eulerian transport is taken as the transport between the time-average posi-  
 149 tion of the bounding surfaces for the layer,

$$U_e = \int_{\bar{\eta}_1}^{\bar{\eta}_2} \mathbf{u} dz, \quad (3)$$

150 here an overbar indicates a time average, leading to  $\bar{\eta}_1$  and  $\bar{\eta}_2$  being the wave-average  
 151 position of the bounding isopycnals. This perspective of calculating transports and fluxes  
 152 within tracer layers has routinely been applied to salt fluxes within estuaries [e.g *Mac-*  
 153 *Donald*, 2006; *MacCready*, 2011].

## 154 2.2 The Stokes' transport for a density layer

155 The Stokes' transport,  $U_s(t)$ , given by the mismatch between the total transport  
 156 and the Eulerian transport,  $U(t) - U_e(t)$ , is now derived following two separations: first  
 157 splitting the velocity and thickness terms into time-mean and time-varying components;  
 158 and secondly separating the vertical averages over the layer into the time-mean extent  
 159 of the layer and the time-varying extent.

160 Firstly, applying a time separation of the time-mean and time-varying components  
 161 to the velocity and layer thickness, the time-mean of the instantaneous volume trans-  
 162 port,  $U(t)$ , is given by

$$\overline{U} = \overline{\langle \mathbf{u} \rangle} \overline{h} + \overline{\langle \mathbf{u} \rangle' h'}, \quad (4)$$

163 made up of the transport from the time-mean flow,  $\overline{\langle \mathbf{u} \rangle}$ , plus the transport from the co-  
 164 variance of the time-varying velocity and layer thickness,  $\overline{\langle \mathbf{u} \rangle' h'}$ , often referred to as the  
 165 bolus transport (Fig. 1a); here the overbar denotes a time average and a prime denotes  
 166 the time-varying deviation with layer-averaged velocity,  $\langle \mathbf{u} \rangle = \overline{\langle \mathbf{u} \rangle} + \langle \mathbf{u} \rangle'(t)$ , and layer  
 167 thickness,  $h(t) = \overline{h} + h'(t)$ .

168 Secondly, the layer-averaged velocity,  $\langle \mathbf{u} \rangle$ , may be separated into the velocity over  
 169 the time-mean extent of the layer,  $\langle \mathbf{u} \rangle_{\overline{h}}$ , plus the velocity following the time-varying move-  
 170 ment of the bounding isopycnals,  $\langle \mathbf{u} \rangle_{h'}$ ,

$$\langle \mathbf{u} \rangle = \langle \mathbf{u} \rangle_{\overline{h}} + \langle \mathbf{u} \rangle_{h'}, \quad (5)$$

171 where  $\langle \mathbf{u} \rangle_{h'}$  gives an implied transport velocity driven by the isopycnal moving through  
 172 velocity shear. Applying this split of the layer-averaged velocities to the total transport  
 173 (4), then leads to the time-mean of the total transport,  $\overline{U}$ , being made up of three terms,

$$\overline{U} = \overline{\langle \mathbf{u} \rangle_{\overline{h}} \overline{h}} + \overline{\langle \mathbf{u} \rangle_{h'} \overline{h}} + \overline{\langle \mathbf{u} \rangle' h'}, \quad (6)$$

174 where the Eulerian transport,  $U_e(t)$ , is given by  $\overline{\langle \mathbf{u} \rangle_{\overline{h}} \overline{h}}$  (the first term on the right-hand  
 175 side) and the Stokes' transport,  $U_s(t)$ , is given by

$$\overline{U_s} = \overline{\langle \mathbf{u} \rangle' h'} + \overline{\langle \mathbf{u} \rangle_{h'} \overline{h}}. \quad (7)$$

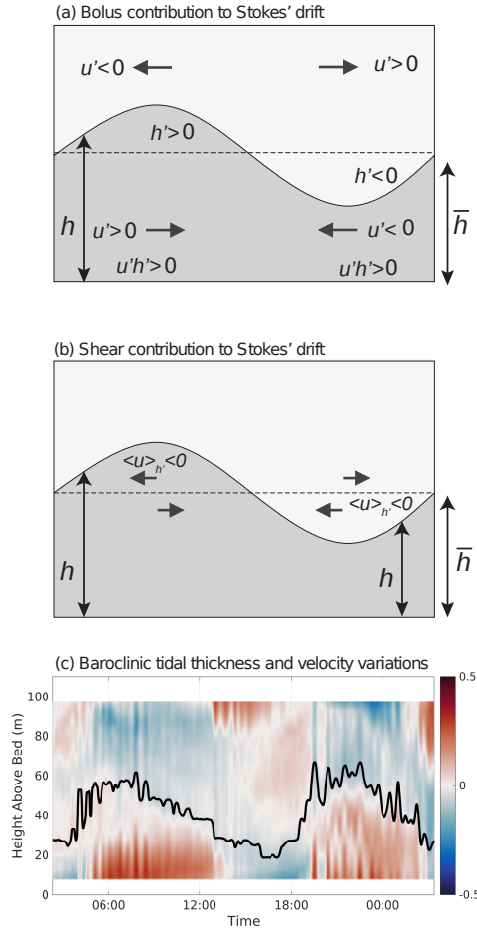
176 The first contribution to the Stokes' transport,  $\overline{\langle \mathbf{u} \rangle' h'}$ , is the co-variance of velocity,  $\mathbf{u}'$ ,  
 177 and layer thickness,  $h'$ , perturbations, often referred to as the bolus transport [Rhines,  
 178 1982]; and the second contribution,  $\overline{\langle \mathbf{u} \rangle_{h'} \overline{h}}$ , represents the time-varying velocity follow-  
 179 ing the movement of the bounding isopycnals,  $\eta'$ , multiplied by the time-mean layer thick-  
 180 ness [McDougall and McIntosh, 2001], referred to as a shear contribution as this con-  
 181 tribution depends on the difference in the velocity following the isopycnal and the ve-  
 182 locity for the layer. This separation of the Stokes;' transport is equivalent to that given  
 183 in McDougall and McIntosh [2001] and was previously explored for an internal wave in  
 184 a lake using temperature coordinates Henderson [2016]. This decomposition of the trans-  
 185 port may not represent the full Lagrangian velocity if there is substantial mixing mod-  
 186 ifying the density structure on time scales shorter than a wave period or if there is large  
 187 horizontal displacements interacting with lateral shear. It is not expected that either of  
 188 these caveats would lead to large errors for this study. The Stokes' transport can alter-  
 189 natively be written as a Stokes' velocity,  $u_s$ , by dividing the transport by the time-mean  
 190 layer thickness,

$$u_s = \frac{\overline{\langle \mathbf{u} \rangle' h'}}{\overline{h}} + \overline{\langle \mathbf{u} \rangle_{h'}}. \quad (8)$$

### 191 2.3 Stokes' transport structure for an internal tide

200 To illustrate the bolus and shear contributions to the Stokes' transport following  
 201 Henderson [2016] consider an internal wave propagating in the positive  $x$  direction. This  
 202 wave leads to oscillating density interfaces and a wave-induced circulation, reversing in  
 203 sign at the mid-depth of the ocean (Fig. 1a,b).

204 For the time-averaged bolus contribution,  $\overline{\langle \mathbf{u} \rangle' h'}$ , in the bottom layer, the layer-  
 205 averaged, time-varying velocity is in the direction of wave propagation,  $u' > 0$ , when  
 206 there is a crest such that the thickness anomaly is positive,  $h' > 0$ , and the bolus trans-  
 207 port per unit length is also positive,  $u' h' > 0$ . As the velocity is reversed in sign,  $u' <$   
 208  $0$ , for a trough, and the thickness anomaly also changes sign,  $h' < 0$ , so that the bolus  
 209 contribution,  $u' h' > 0$ , remains positive over the entire wavelength (Fig. 1a). For



192 **Figure 1.** The transport from the Stokes' drift is made up of two contributions (7): (a) the  
 193 bolus contribution driven by the co-variance of layer thickness and the velocity within the layer;  
 194 and (b) the shear contribution from the correlation of the vertical shear in the horizontal velocity  
 195 and the height of the moving isopycnal. The grey arrows denote the direction of the depth-mean  
 196 velocity in (a) and the velocity shear in (b). This schematic is comparable to Figure 4 in *Hen-*  
 197 *derson* [2016]. In (c), the internal tide leads to an onshore bolus contribution from the onshore  
 198 velocity being correlated with greater layer thickness in the top and bottom layers, illustrated  
 199 here using observed velocities from a mooring on the New Zealand shelf.

210 the bolus contribution in the upper layer, a similar phase relationship holds between ve-  
 211 locity and layer thickness, so that  $u'h' > 0$  is again positive.

212 For the time-averaged shear contribution,  $\overline{\langle \mathbf{u} \rangle_{h'} \bar{h}}$ , the time-varying velocity follow-  
 213 ing the interface is negative for both the crest and the trough. In the crest, the positive  
 214 height displacement coincides with a negative vertical shear in horizontal velocity to give  
 215 a negative velocity averaged along the interface,  $\langle u' \rangle_{h'} < 0$ . In the trough, the nega-  
 216 tive height displacement coincides with a positive vertical shear in horizontal velocity  
 217 and gives a negative velocity averaged along the interface,  $\langle u' \rangle_{h'} < 0$  (Fig. 1b).

### 218 3 Model assessment of the Stokes' drift for an internal tide

219 The vertical structure of the Stokes' drift and its bolus and shear contributions are  
 220 next illustrated using a pair of highly idealised model experiments. The aim of these ex-  
 221 periments are to illustrate the application of the layered analysis set out in Section 2 and  
 222 to consider the impact of the choices of layers on the calculated transports.

#### 223 3.1 Model setup

224 The Stokes' drift for an internal tide over a flat bottom is now examined using a  
 225 Massachusetts Institute of Technology General Circulation Model [MITgcm, *Marshall,*  
 226 1997] simulation. The model is configured in a two-dimensional channel, in the vertical  
 227 and direction of wave propagation; with a domain 200 km long and 1000 m deep, and  
 228 with horizontal and vertical resolutions of 250 m and 20 m, respectively. The model has  
 229 a flat bottom with no shelf or slope. The model is integrated in non-hydrostatic mode  
 230 with a linear free surface condition for two cases: one without rotation and one with ro-  
 231 tation ( $f = 10^{-4} \text{ s}^{-1}$ ). Viscosity and horizontal diffusivity are uniform ( $\nu_h = 10^{-2} \text{ m}^2 \text{ s}^{-1}$ ,  
 232  $\nu_z = 10^{-3} \text{ m}^2 \text{ s}^{-1}$ , and  $\kappa_h = 10 \text{ m}^2 \text{ s}^{-1}$ ); vertical diffusivity is calculated using a con-  
 233 vective adjustment [*Legg and Adcroft, 2003*].

234 Initial conditions are no flow, uniform salinity and a linear temperature profile lead-  
 235 ing to horizontally-uniform stratification ( $N^2 = 5 \times 10^{-6} \text{ s}^{-2}$ ) using a linear equation  
 236 of state. Boundary conditions are no slip at the bottom, no stress at the surface, and  
 237 no buoyancy flux at either the surface or the bottom boundaries. Oscillating velocities  
 238 and temperature anomalies are prescribed at the western boundary following *Legg and*  
 239 *Adcroft* [2003] and *Hall et al.* [2013] and force an eastward propagating internal tide for  
 240 mode-1,  $M_2$  ( $\omega = 1.4 \times 10^{-4} \text{ s}^{-1}$ ) with an amplitude,  $a = 14 \text{ m}$ , and horizontal wave-  
 241 length,  $\lambda = 30 \text{ km}$ , and phase speed,  $c = 0.67 \text{ m s}^{-1}$ . This boundary forcing has no  
 242 net depth averaged transport however would allow a Lagrangian transport at individ-  
 243 ual depths, consistent with an internal tide. The temperature is relaxed to the initial con-  
 244 ditions from the mid-point of the model (100 km) to the eastern boundary. This relax-  
 245 ation is ramped up towards the boundary with a hyperbolic tangent function in order  
 246 to dissipate internal waves without reflection. This relaxation allows volume to be ex-  
 247 changed between density classes allowing a net transport within layers. The model is run  
 248 for 12 tidal cycles ( $12T$ ) and the forcing ramped up over the first two tidal cycles to avoid  
 249 transients.

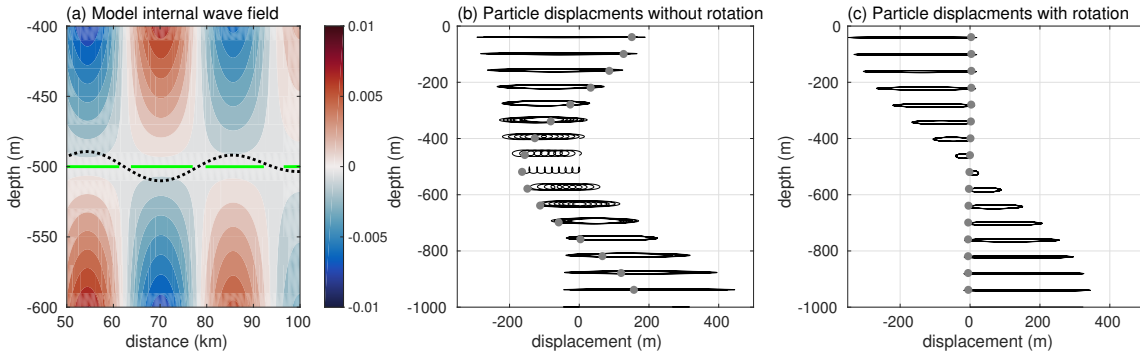
250 The diagnostics of the Stokes' drift transport is only applied in the interior of the  
 251 domain, from 10 km to 30 km, and over time intervals from  $4T$  to  $12T$ , chosen so that  
 252 the boundaries and ramping of the forcing does not influence the results.

255 The Stokes' transport,  $\overline{U_s}$ , within density layers is diagnosed for the internal tide  
 256 in two ways for the two-dimensional model:

257 1. The model is seeded with 50 particles and their displacements are tracked us-  
 258 ing a 4th-order Runge-Kutta scheme;

253 **Table 1.** Table of parameters used in the setup and analysis of the idealised two-dimensional  
 254 model.

| Parameter                  | Value                            |
|----------------------------|----------------------------------|
| Domain length              | 200 km                           |
| Horizontal resolution      | 250 m                            |
| Domain depth               | 1000 m                           |
| Vertical resolution        | 20 m                             |
| Run time                   | 12 $M_2$ cycles                  |
| Time step                  | 60 seconds                       |
| Buoyancy frequency squared | $5 \times 10^{-6} \text{s}^{-2}$ |
| Diagnostic subdomain       | 10-30 km                         |
| Diagnostic time period     | 4 to 12 $M_2$ cycles             |



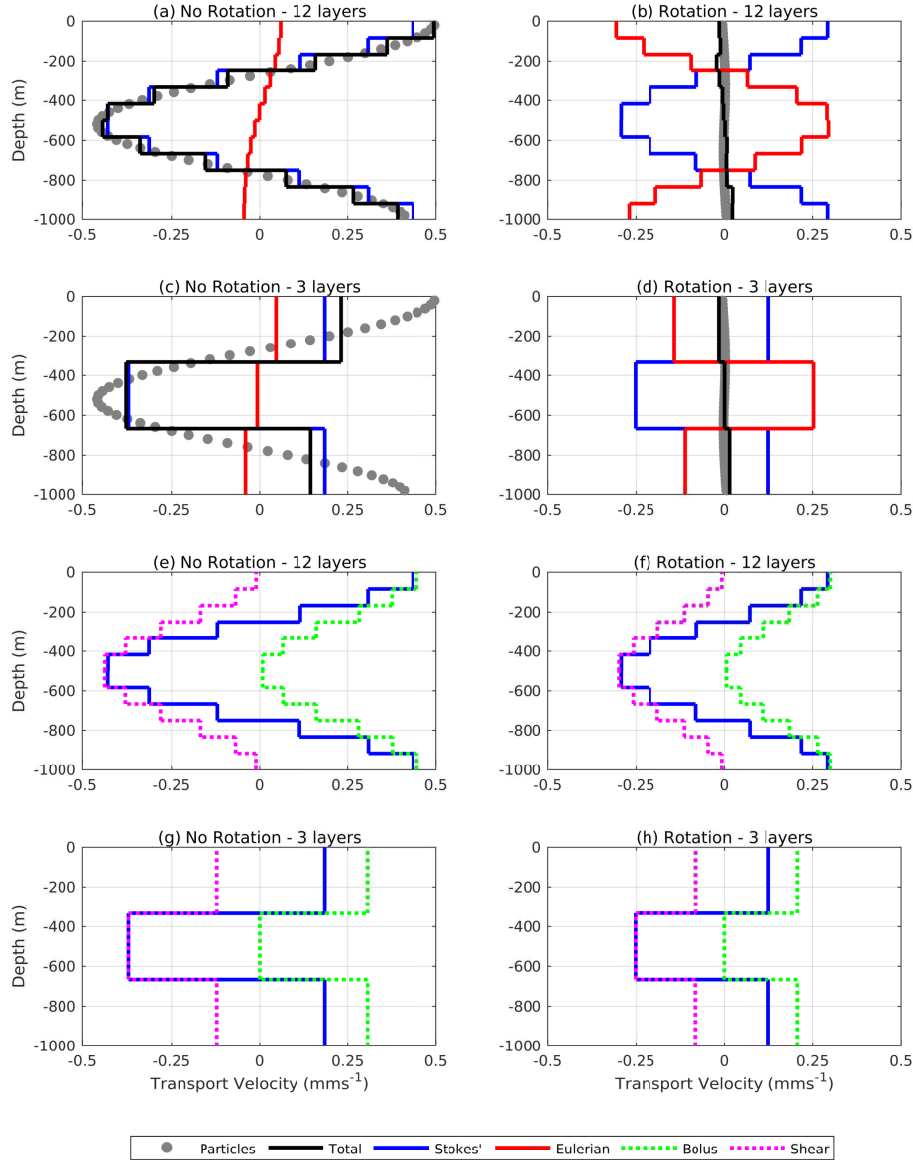
263 **Figure 2.** (a) Model subsection of mode 1, internal tide with undulations in temperature  
 264 surfaces (black), the zero crossing of velocity (green) and zonal velocity ( $\text{m s}^{-1}$ ) in an idealised  
 265 two-dimensional model with constant  $N^2$ ; and model illustration of Lagrangian particle dis-  
 266 placements over 8 wave periods (with final positions marked by grey circles) from the model (b)  
 267 without rotation and (c) with rotation.

259 2. The shear transport,  $\overline{\langle \mathbf{u} \rangle_h' h}$ , and the bolus transport,  $\overline{\langle \mathbf{u} \rangle' h'}$ , contributions are  
 260 evaluated for a different number of layers, and their sum provides an estimate of  $\overline{U_s}$  for  
 261 each layer (7).

### 262 3.2 Particle drift versus layered transport

274 The internal tide leads to the particles oscillating back and forth for both the non-  
 275 rotating and rotating cases (Fig. 2b,c). Over repeated tidal periods, there is a system-  
 276 atic displacement of particles in the non-rotating case, the particles are transported in  
 277 the direction of the internal tide propagation close to the surface and the bottom, but  
 278 are transported in the opposite direction at mid depths (Fig. 2b). However, in the ro-  
 279 tating case, the particles are not systematically displaced by the internal tide due the  
 280 Eulerian velocity (Fig. 2c). This vertical structure for the Stokes' velocity and its con-  
 281 tributing components is in agreement with previous theoretical work [Thorpe, 1968].

282 When using 12 layers, the total transport in layers without rotation is positive near  
 283 the boundaries and negative at mid depths (Fig. 3a, black line). The total transport in  
 284 the model run with rotation is small at all depths (Fig. 3a, black line). This response  
 285 is consistent with the particle displacements in both vertical structure and magnitude



268 **Figure 3.** The vertical structure of the transport velocity derived from the particle displacements (grey circles), the total transport (black line), the Stokes' transport (blue line), the Eulerian transport (red line), the bolus contribution to the Stokes' transport (dashed green line), and the shear contribution to the Stokes' transport (dashed magenta line). The transports have been calculated for two different choices for the number of layers: (a,b,e,f) 12 layers, and (c,d,g,h) 3 layers, and for both non-rotating (a,c,e,g) and rotating (b,d,f,h) cases.

269  
270  
271  
272  
273

(Fig. 3a,b, black lines and grey circles). This agreement illustrates the ability of the layered analysis to diagnose the Lagrangian transport, as previously shown theoretically [e.g. *McDougall and McIntosh, 2001*].

With a reduction in the number of layers, the overall vertical structure of the Stokes' drift driven by a mode-one internal wave is retained with a minimum of three layers, although there is a reduction in the vertical detail of the particle advection (Fig. 2c,d, black line and grey dots). Whilst the three layer approach captures the average particle displacement and volume transport within the layers well, the accuracy of the diagnosed maximum transport is increased when using an increased number of layers. For example, for the bottom of the 3 layers the total Stokes' transport velocity without rotation is  $0.19 \text{ mms}^{-1}$  whilst the equivalent four layers within the 12 layer calculation have an average transport velocity of  $0.18 \text{ mms}^{-1}$ .

### 3.3 Cancellation of the Stokes' transport by the Eulerian transport

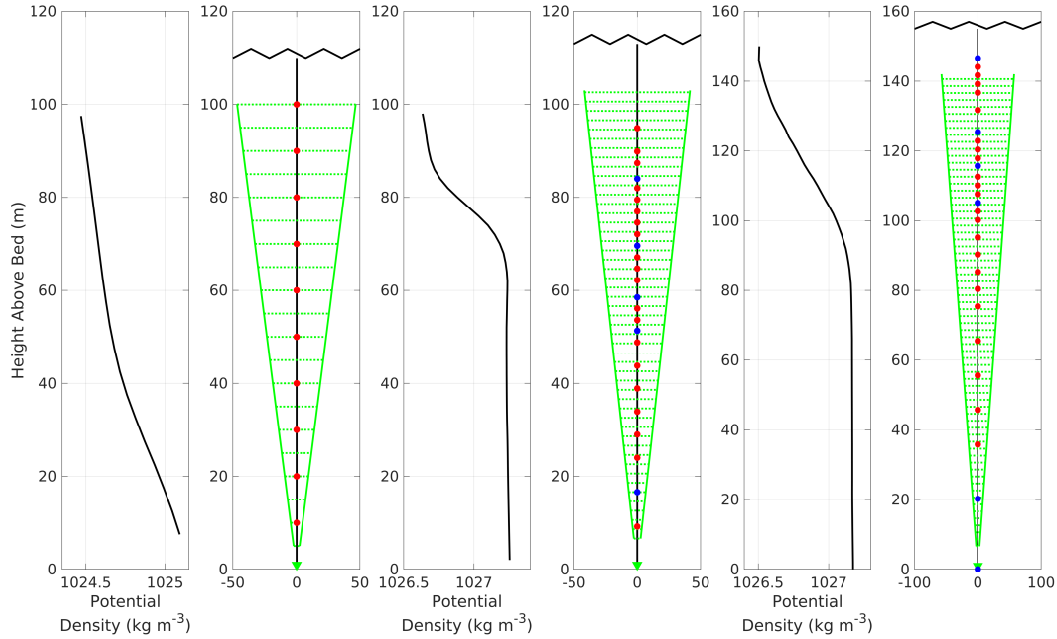
In both the non-rotating and rotating cases, the Stokes' transport is in the direction of the internal wave propagation near the boundaries and in the opposite direction at mid depths (Fig. 3a,b, blue lines). In the non-rotating case, there is a weak Eulerian transport, so that the Stokes' transport is the main contributor to the total transport (Fig. 3a). In the rotating case, the Stokes' transport has the same vertical structure as in the non-rotating case, although it is 32% weaker. However, the Eulerian transport is now comparable in magnitude to the Stokes' transport in all layers, but with the opposite sign. Consequently, the total transport from the sum of the Eulerian and Stokes' transports is relatively small, consistent with previous theoretical studies for an inviscid ocean [*Wagner and Young, 2015*]. These theoretical and modelling results however need not hold for the real ocean due to a variety of reasons: spatial inhomogeneity in the internal tide field, leading to non-local return flows; temporal variability in the Stokes' transport leading to periods of enhanced transport; or strong turbulent mixing on the shelf driving diapycnal exchange between layers. The extent of the cancellation of the Stokes' transport by Eulerian flows will be tested in observations in Section 4.

### 3.4 Contributions to the Stokes' transport

The Stokes' velocity is made up of a bolus contribution and a shear contribution [*McDougall and McIntosh, 2001*]. The bolus contribution is in the same direction as the propagation of the wave and is a maximum at the boundaries for both the non-rotating and rotating cases (Fig. 3e,f, green dashed lines). The shear contribution is in the opposite direction to the wave propagation and is a maximum at mid depths (Fig. 3e,f, magenta dashed lines). The combination of these two terms gives rise to (i) the Stokes' transport in the direction of internal-wave propagation near the boundaries, where the bolus transport dominates, and (ii) the Stokes' transport opposing the direction of internal-wave propagation at mid depths, where the shear transport dominates [*Henderson, 2016*].

## 4 Stokes' transport diagnosed from current moorings

The Stokes' transport is now diagnosed for three different moorings on the continental slope. The transports are evaluated within 3 layers from the moorings. Our expectation is that the internal tide provides a bolus transport, with a component directed from the continental slope towards the shelf seas, which is returned at mid depth by an opposing shear contribution. The extent of the cancellation between the Stokes' transport and Eulerian-mean transport is also assessed.



338 **Figure 4.** A series of density profiles and mooring diagrams for: (a) and (b) the New Zealand  
 339 (NZ); (c) and (d) the Malin Shelf (SG); and (e) and (f) the Celtic Sea (ST4) moorings. The  
 340 density profiles (a), (c) and (e) show the average density profile from the moorings. The moor-  
 341 ing diagrams (b), (d) and (f) show the ACP data in green with the triangle showing the ADCP  
 342 position, the solid green lines the spread of the pings and the dashed lines the boundaries of the  
 343 ADCP bins. The solid circles show the temperature sensors in red and the temperature and  
 344 conductivity sensors in blue.

#### 331 4.1 Moorings sites

332 Three different near shelf-break internal tide regimes have been observed using moor-  
 333 ings. At New Zealand the shelf break is smooth and, although the barotropic forcing is  
 334 weak, there is a strong internal tide propagating from the slope onto the shelf. At the  
 335 Malin Shelf, the shelf break is again smooth, although there are only weak internal tides.  
 336 Finally, in the Celtic Sea, the internal wave field is more complex due to the corrugated  
 337 topography at the shelf edge and the proximity of the mooring to a spur in the shelf edge.

##### 345 4.1.1 New Zealand shelf

346 One mooring was deployed on the north-east New Zealand shelf for approximately  
 347 13 days in 110 m of water during November and December 1998. The mooring consisted  
 348 of a near-bed upward looking 500 kHz Acoustic Current Profiler (ACP) and a string of  
 349 10 temperature loggers with a constant separation of 10m [Sharples *et al.*, 2001]. The  
 350 ACP used 1 minute ensembles and 5 m vertical bins with first bin 5m from the bottom  
 351 and the bins 10 m or less from the surface removed (Fig. 4b). The temperature and cur-  
 352 rent data were linearly interpolated onto a 1 minute x 5 metre resolution grid. Salinity  
 353 was taken from a single nearby CTD station. The water column was stratified (Fig. 4a),  
 354 although the stratification was weakened by a wind mixing event at days 4 to 5. Due to  
 355 the weakened stratification the analysis has only been performed over the 7 days after

356 stratification has recovered. This 7 day period covers the transition from neap to spring  
357 tide.

358 The baroclinic energy flux is calculated from the mooring data from the wave per-  
359 turbations of pressure and velocity following *Nash et al.* [2005]; using a high-pass But-  
360 terworth filter to remove sub-tidal frequencies in the mooring data with a cut off of  $1.25/\omega_{M2}$ ,  
361 where  $\omega_{M2}$  is the M2 tidal frequency. There is a strong baroclinic energy flux directed  
362 onto the shelf, which is modified by the weakening stratification [*Sharples et al.*, 2001].

#### 363 **4.1.2 European Malin shelf**

364 A mooring, SG, was deployed on the north-west European Malin Shelf for approx-  
365 imately 15 days in 117 m of water during July 2013. Over the full water column, the tem-  
366 perature structure was recorded by a string of 20 temperature loggers and 6 CTDs. These  
367 instruments ranged from 18 m to 116 m depth with a minimum spacing of 2.5 m at the  
368 pycnocline and a maximum spacing of 13 m near the bed (Fig. 4c,d). The currents were  
369 recorded by an upward looking Flowquest 150 kHz ACP mounted in a bed frame [*Short*  
370 *et al.*, 2013]. The ACP employed a 1 minute ensemble that consisted of 60 pings. The  
371 vertical bin size was 2m with the first bin 6.6 m from the bed and the surface 13 m re-  
372 moved due to side lobe contamination. The salinity and density profiles were constructed  
373 from 6 CTDs deployed on the mooring [*Hopkins et al.*, 2014]. All measurements were  
374 linearly interpolated onto coincident 1 minute x 2 metre grids. The water column was  
375 well stratified throughout the observational period (Fig. 4c) and showed a weak and per-  
376 sistent baroclinic energy flux propagating onshore. The mooring period captures a full  
377 spring neap cycle.

#### 378 **4.1.3 European Celtic Sea shelf**

379 A mooring, ST4, was deployed in the Celtic Sea on the north-west European Shelf  
380 for approximately 12 days in 156 m of water respectively. The mooring consisted of a  
381 bed-mounted Flowquest 150 kHz ACP, with the same setup as for SG with the upper  
382 10 m removed, and a string of 22 temperature loggers and 7 CTDs. The temperature  
383 loggers and CTD's ranged from 9 m to 155 m depth with a minimum spacing of 2.5 m  
384 in the pycnocline and a maximum spacing of 20 m near the bed (Fig. 4e,f). Observa-  
385 tions were interpolated onto a full water column 1 minute x 2 metre grid. There was a  
386 strong wind event shortly after deployment that significantly modified the density struc-  
387 ture of the water column [*Hopkins et al.*, 2014; *Stephenson Jr. et al.*, 2015] and drove  
388 strong residual surface currents. The time series is trimmed to the 8 days after the storm  
389 when the water column is stratified, as that period is more representative of typical sum-  
390 mer conditions. This period captures the transition from spring to neap tides. In this  
391 region, the shelf break is heavily canyoned, which results in a strong and highly variable  
392 internal wave propagation [*Vlasenko et al.*, 2014]. During the mooring deployment, the  
393 baroclinic energy flux at the mooring location was directed along slope.

## 394 **4.2 Diagnostic method**

395 Our aim is to identify the Stokes' transport (8) connected to the propagation of  
396 the internal tide from the continental slope onto the shelf. This assessment is based on  
397 an analysis of three separate sets of moorings. Our expectation based on the theory and  
398 model simulation is that the Stokes' velocity is directed onshore near the surface and the  
399 bottom, and returned offshore in the pycnocline.

400 The transport for the moorings is diagnosed for three density layers with their in-  
401 terfaces defined by the surface, bed and the zero crossings of the theoretical baroclinic  
402 mode-1 Stokes' drift. This theoretical vertical structure is taken from *Thorpe* [1968] with  
403 the modal structure calculated from the averaged density profile from the moorings [*Klink*,

1999]. Time averaging is applied by taking the time-mean depth of isopycnals, rather than the time-mean density at a fixed depth, and so avoids spurious smearing of the pycnocline due to internal waves. The time span used for time-averaging of transports are chosen to extend over an integer number of M2 periods in order to reduce aliasing. The velocity and density outside the part of the water column covered by the observations are estimated by extrapolation to the boundary.

Two sources of error are considered in these calculations: firstly the error in the horizontal velocities provided by the ACP, and secondly the error in estimating the thickness of layers due to the positioning of the instruments. The ACP error is taken as 1% of the recorded velocity plus  $5 \text{ mm s}^{-1}$  following the manufacturers guidelines [LinkQuest Inc., 2007]. Here we have applied this error by taking a maximum velocity of  $1 \text{ m s}^{-1}$ , larger than the barotropic tidal magnitude at all sites, giving an error of  $1.5 \text{ cm s}^{-1}$ . The error in the separation between the barotropic and baroclinic components was estimated by performing the split using the current only within the depth range the ACP observed directly and extrapolating the velocities to the boundary. The error from this source was less than the error implied by the manufacturer tolerances, less than  $1 \text{ cm s}^{-1}$  in all moorings. The resulting total velocity error is  $2.5 \text{ cm s}^{-1}$ . The error in layer thickness is taken as the the separation between the instruments at the location of the pycnocline, 5 m for NZ and 2 m for SG and ST4. These errors are then carried through the calculation of transport using a Monte Carlo approach. We assume that the errors are normally distributed with a standard deviation to match the magnitudes above and then generate 1000 realisations of each time-series with a normally distributed pseudo-random error added.

### 4.3 Time series of Stokes' transport

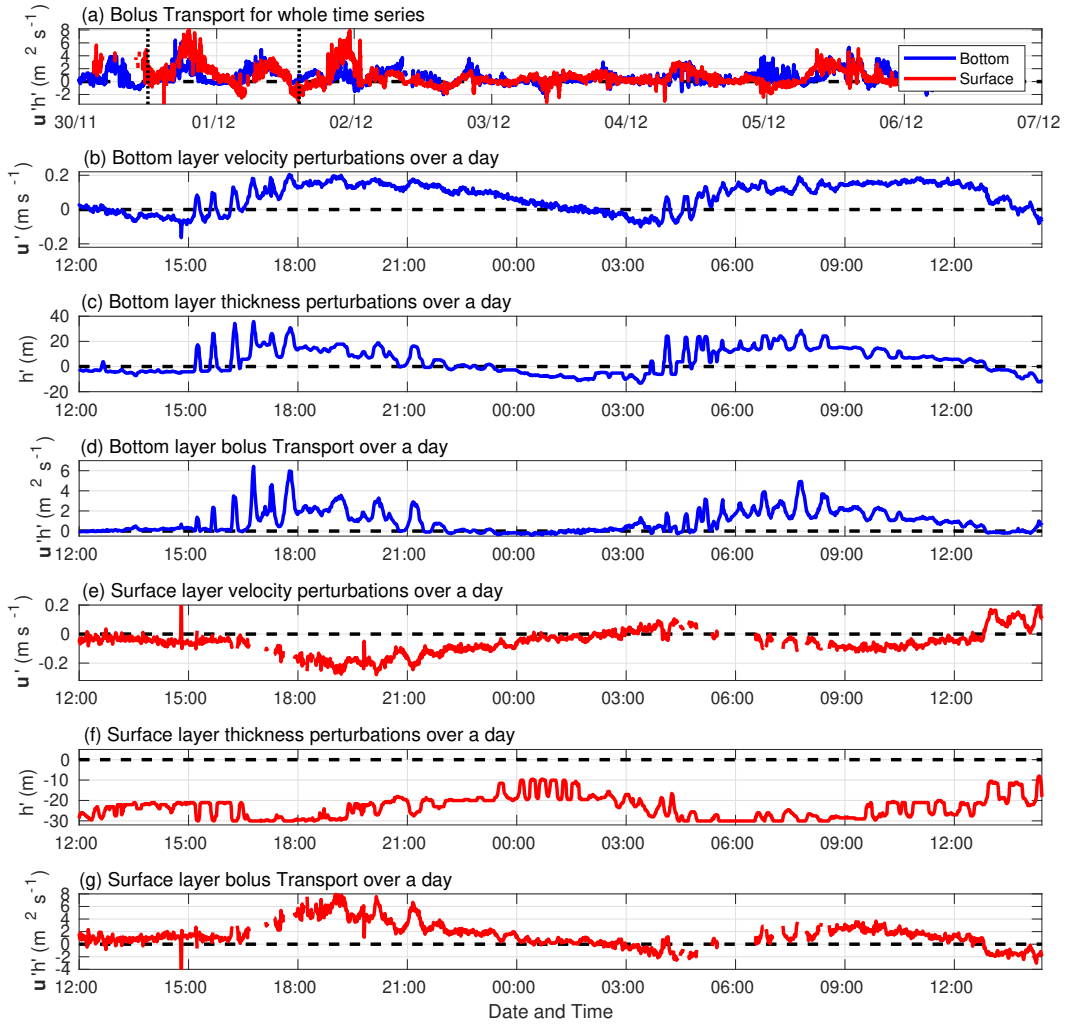
The Stokes' transport and its contributions have been evaluated for the New Zealand mooring for the time series from 30 November to 6 December 1998. The time series of these terms are presented for the whole mooring period and a selected day to highlight the dominant processes.

#### 4.3.1 Bolus transport

In the bottom layer, the bolus transport is directed on shelf and is positive throughout much of the time series (Fig. 5a), in accord with the direction of internal-wave propagation. This positive contribution is due to the bottom velocity and thickness of the bottom layer being in phase. There is a dominant M2 tidal signal in both the thickness and velocity terms (red and blue in Fig. 6c) that are in phase with each other leading to a net transport with an M2 period (black in Fig. 6d). There is an asymmetry in this contribution between the periods when the isopycnals are above and below their mean depths leading to an M2 period in the resultant bolus transport (black in Fig. 6d). In addition to this M2 tidal signal, there is an additional volume transport driven by short period non-linear internal waves on the leading edge of the internal tide (Fig. 5b,c,d). A similar M2 period signal is seen in the bolus transport for the surface layer (Fig. 5e,f,g and Fig. 6a,d) however the layer is thinner than the mean thickness and the spectra show additional long period variability with the opposite phase relation in the velocity and bolus transport, likely due to surface forcing.

#### 4.3.2 Shear transport

The shear-driven transport in the middle layer is negative through much of the time series (Fig. 7a). This negative transport is due to the negative shear driven transport velocity (the difference between the blue and red lines in Fig. 7b). This signal is revealed by considering the sign of the displacement of the boundaries of the layer and the vertical shear in velocity. When the boundaries are displaced upward, with a positive isopy-



447 **Figure 5.** Time series showing the contributions to the bolus transport in the direction of the  
 448 baroclinic energy flux per unit horizontal length,  $u'h'$  ( $\text{m}^2\text{s}^{-1}$ ) in the surface and bottom layer  
 449 at the New Zealand mooring: (a) the full time series of instantaneous bolus transport,  $u'h'$ , with  
 450 the selected day shown with vertical dotted lines, (b) the bottom layer velocity perturbations,  
 451  $u'$  ( $\text{m s}^{-1}$ ) in the direction of the baroclinic energy flux for a selected day, (c) the bottom layer  
 452 thickness perturbations,  $h'$  (m) for a selected day, and (d) the bottom layer bolus transport,  $u'h'$ ,  
 453 for a selected day, (e) the surface layer velocity perturbations,  $u'$  ( $\text{m s}^{-1}$ ) in the direction of the  
 454 baroclinic energy flux for a selected day, (f) the surface layer thickness perturbations,  $h'$  (m) for  
 455 a selected day, and (g) the surface layer bolus transport,  $u'h'$ , for a selected day. The gaps in the  
 456 surface layer are where the isopycnal was shallower than the most shallow instrument and thus  
 457 no data was collected for the layer.

464 cnal displacement, the velocity is negative higher in the water column so that there is  
 465 a negative vertical shear in velocity (Fig. 7c,d). This contribution leads to the velocity  
 466 averaged along the isopycnal to be biased negative when compared to the average ve-  
 467 locity at the mean position of the isopycnal (Fig. 7e). The product of the layer averaged  
 468 shear and displacements agrees well with the shear driven transport velocity (red and  
 469 blue lines respectively in Fig. 7e). This signal is present in both the average shear and  
 470 isopycnal displacement of the middle layer with an M2 period (blue and red in Fig. 6b)  
 471 which is now in opposite phase to each other leading to a net negative transport (red in  
 472 Fig. 6d which is plotted with the opposite sign). As with the bolus transport, there is  
 473 an asymmetry in the shear transport between the phases of the internal tide leading to  
 474 an M2 period in the resultant shear driven transport velocity (red in Fig. 6d). Here the  
 475 shear transport is larger when the internal tide is leading to isopycnals being elevated  
 476 above their mean depth compared to the phase when the isopycnals are below their mean  
 477 position.

#### 497 **4.4 Direction and vertical structure of Stokes' transport**

498 Now the time-averaged Stokes' transport, and its contributions, within three lay-  
 499 ers, are considered for all three moorings, as well as assessing the extent that the Eu-  
 500 lerian transport cancels the Stokes' transport.

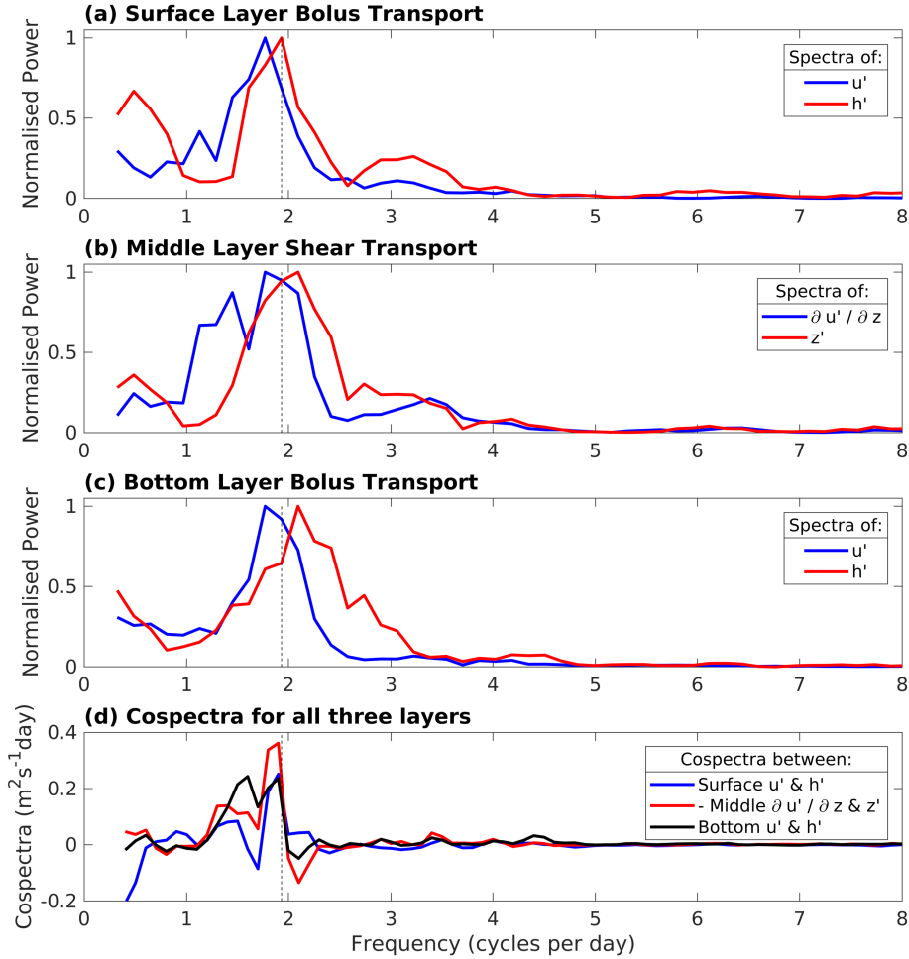
##### 501 **4.4.1 New Zealand shelf**

502 On the New Zealand Shelf, the internal tide is strong, compared to the other sites  
 503 considered here, and is directed onto the shelf (Fig. 8a). The depth-integrated bolus trans-  
 504 port is in the same direction as the baroclinic energy flux (Fig. 8b). The shear trans-  
 505 port is approximately the same magnitude as the bolus transport, but is in the oppo-  
 506 site direction (Fig. 8c). For both of these contributions the error implied in the obser-  
 507 vations is much smaller than the magnitude of the transport. The combination of these  
 508 two components leads to a depth-integrated Stokes' transport that is indistinguishable  
 509 from zero when including the observational error (Table 2).

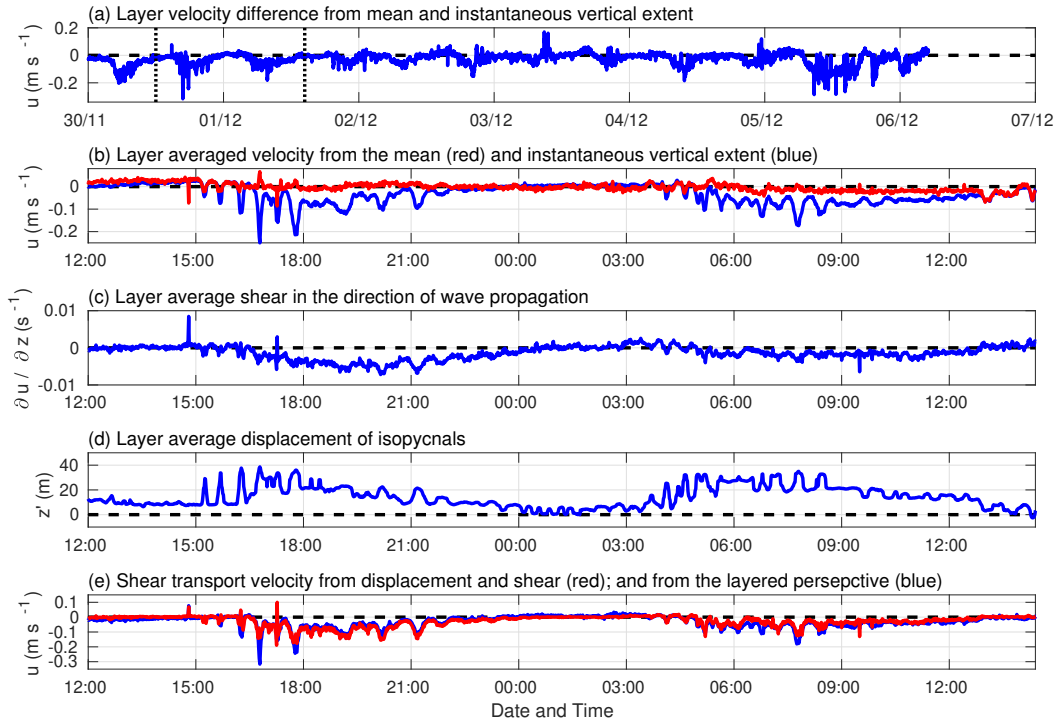
510 Now consider the vertical structure of the transport based upon a separation into  
 511 three layers. The bolus transport is strong and in the direction of the baroclinic energy  
 512 flux in the surface and bottom layers, whilst the bolus transport is weak in the middle  
 513 layer (Fig. 8b). The shear transport is strong and opposes the direction of propagation  
 514 in the middle layer, whilst the surface and bottom layers have weak transport (Fig. 8c).  
 515 These contributions lead to a Stokes' drift that is strongest in the middle layer and in  
 516 the opposite direction to the propagation of the wave, whilst the surface and bottom lay-  
 517 ers have weaker transport directed in the same direction as the energy flux (Fig. 8d).  
 518 This response is consistent with the vertical structure of the Stokes' transport given by  
 519 the theory and modelling, with bolus dominating near the boundaries and the shear dom-  
 520 inating at mid depth (Fig. 8d). On the New Zealand shelf, the Eulerian transport is sim-  
 521 ilar in magnitude to the Stokes' transport, but is primarily directed along the bathymet-  
 522 ric contours (Fig. 2b). Hence, there is no implied cancellation of the Stokes' transport  
 523 onto the shelf by the Eulerian transport.

##### 535 **4.4.2 European Malin shelf**

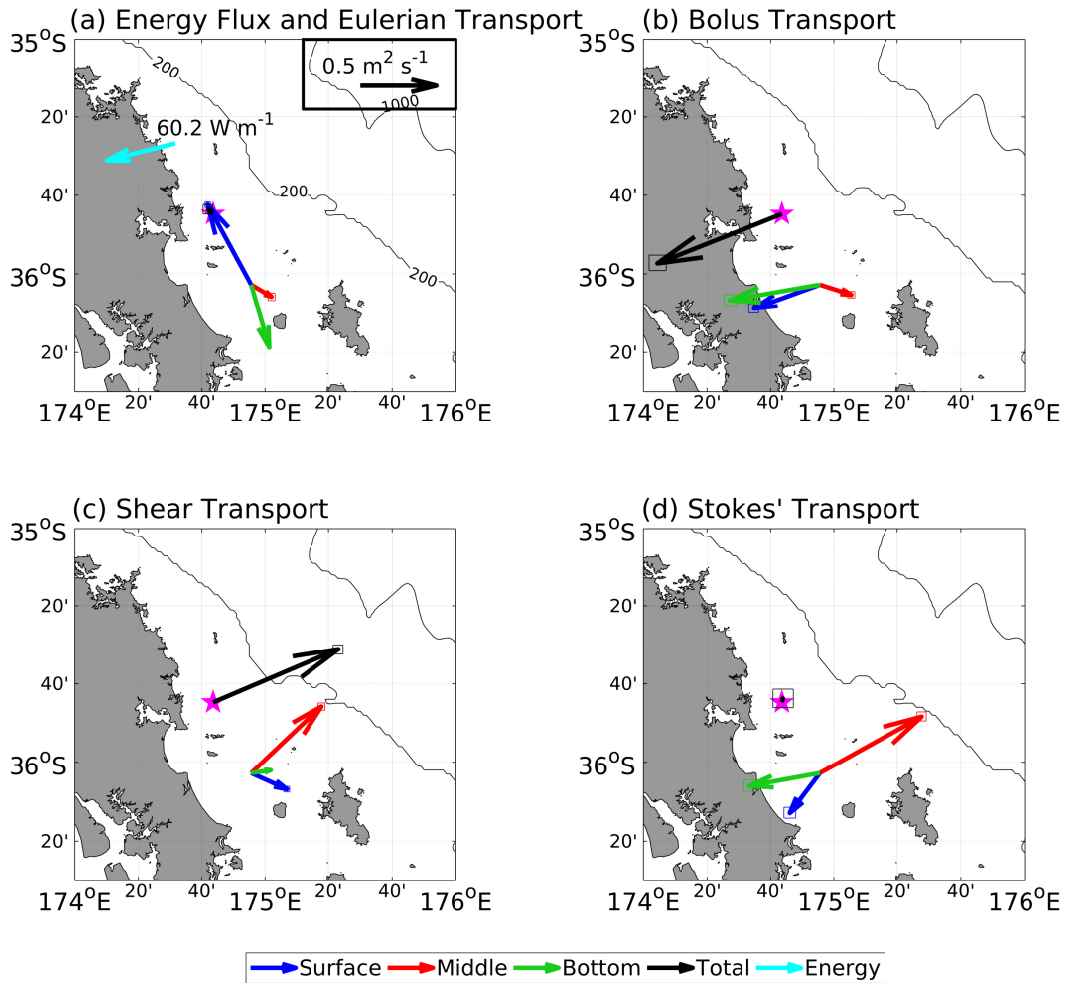
536 On the Malin Shelf, the internal tide again propagates onto the shelf, although it  
 537 is an order of magnitude weaker than on the New Zealand Shelf (Fig. 9a). The layered  
 538 Stokes' transport shows the same structure as for the mooring on the New Zealand shelf  
 539 (Fig. 9b,c,d), consistent with the expected bolus and shear contributions, although in  
 540 the bottom layer the error estimate is larger than the calculated transport (Table 2). The  
 541 resulting depth-integrated transport is very small, smaller than the 99 % confidence in-  
 542 tervals so the transport is statistically indistinguishable from zero (Table 2). On the Ma-



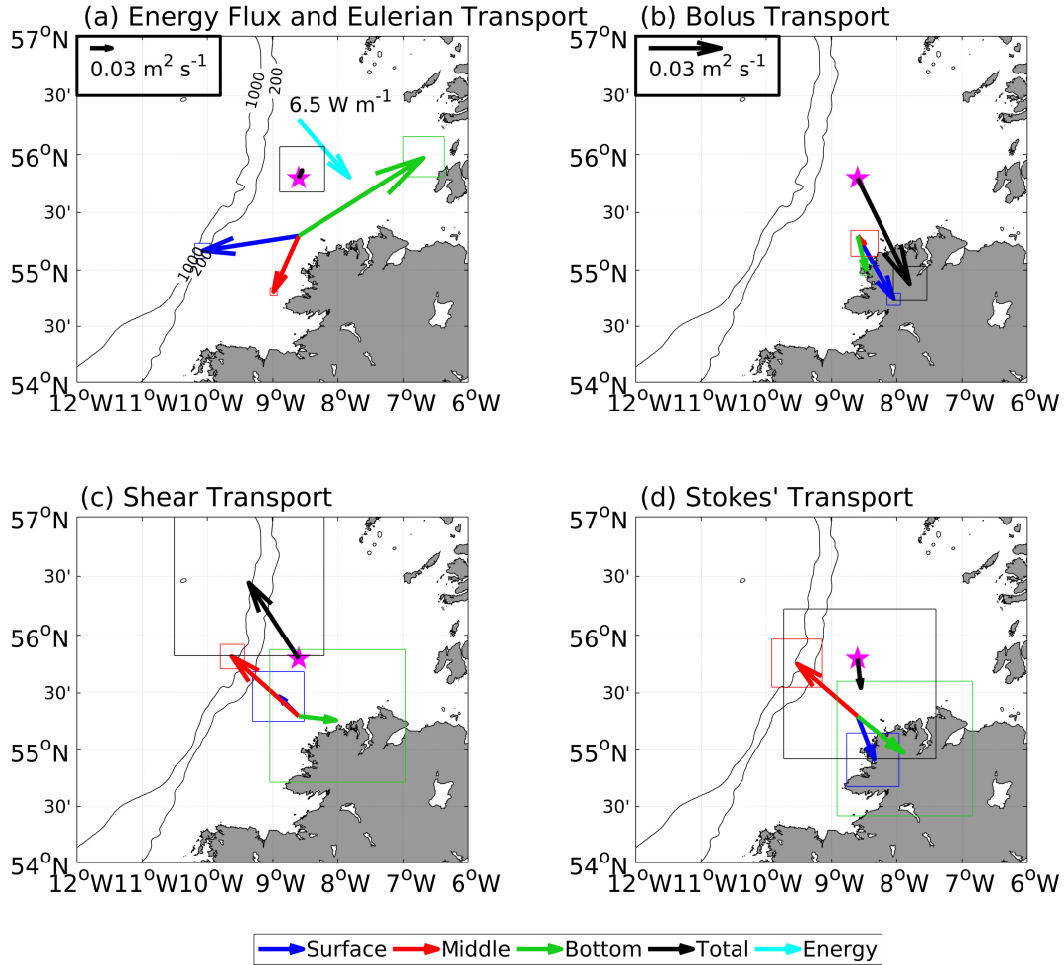
478 **Figure 6.** Power spectra and co-spectra of the leading contributions to the Stokes' transport  
 479 for each layer. Each power spectra is normalised by its maximum value. The bolus transport is  
 480 shown for the (a) surface and (c) bottom layer with the blue line showing the velocity perturba-  
 481 tions and the red line showing the thickness perturbations. The shear transport is shown for (b)  
 482 the middle layer with the blue line showing the layer average shear and the red line showing the  
 483 layer average displacement. The co-spectra are shown (d) between: the thickness and velocity  
 484 perturbations for the surface (blue line) and bottom (black line) layers; and the layer average  
 485 shear and vertical displacement, scaled by the average layer thickness, for the middle layer (red  
 486 line). The sign of the middle layer co-spectra is reversed. The vertical dashed line is the M2 tidal  
 487 period.



488 **Figure 7.** Time series showing the contributions to the shear transport for the middle layer in  
 489 the direction of the baroclinic energy flux per unit horizontal length for the New Zealand moor-  
 490 ing: (a) the difference between the velocity depth averaged over the mean extent of the layer and  
 491 the instantaneous extent over the whole time series ( $\text{ms}^{-1}$ ), (b) the velocity depth averaged over  
 492 the mean, red, and instantaneous, blue, extents over a selected day ( $\text{ms}^{-1}$ ), (c) the average shear in  
 493 the middle layer ( $\text{s}^{-1}$ ), (d) the average displacement of isopycnals in the middle layer (m), and  
 494 (e) the implied shear transport given by the product of the shear and isopycnal displacment in  
 495 red and the difference between the velocity depth averaged over the mean extent of the layer and  
 496 the instantaneous extent.



524 **Figure 8.** Baroclinic energy flux ( $\text{W m}^{-1}$ ), Stokes' transport, and contributions per unit  
 525 horizontal length ( $\text{m}^2\text{s}^{-1}$ ) on the New Zealand Shelf. (a) The baroclinic energy flux and the  
 526 transport driven by: (a) the time-mean Eulerian transport, (b) the time-mean bolus contribution  
 527 from the correlation of velocity and layer thickness, (c) the time-mean shear contribution eval-  
 528 uated from the departures from the time-mean isopycnal depth, and (d) the Stokes' transport  
 529 from the sum of the bolus and shear contributions. The calculations have been performed over  
 530 multiple layers: the surface (blue), the middle (red), the bottom (green), and over the whole wa-  
 531 ter column (black). The layered transport is offset from the mooring location to make the figure  
 532 easier to read. The position of the mooring is marked with the magenta star. The rectangle sur-  
 533 rounding the head of each arrow indicates 99% of the Monte Carlo realisations representing the  
 534 error in the observations, as described in Section 4.2.

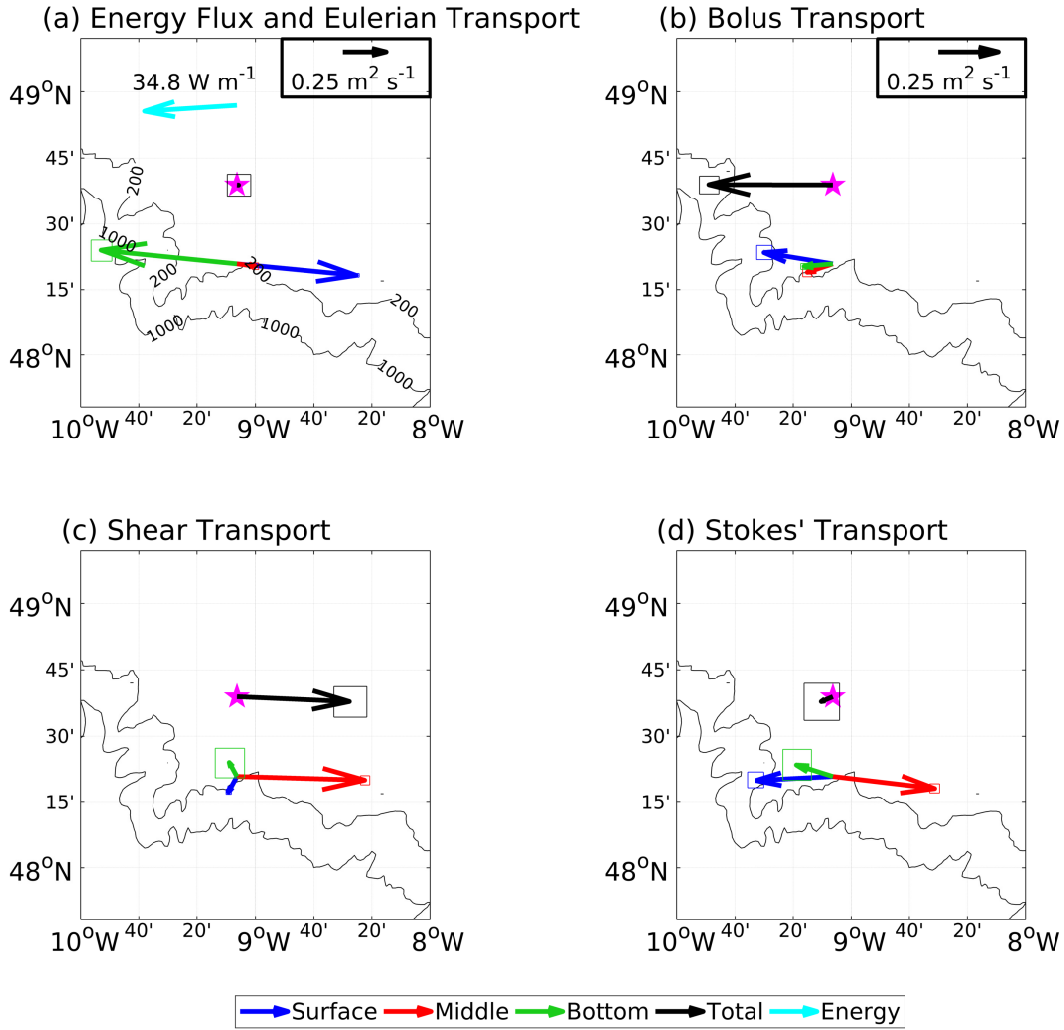


547 **Figure 9.** Baroclinic energy flux ( $\text{W m}^{-1}$ ), Stokes' transport, and contributions per unit  
 548 horizontal length ( $\text{m}^2 \text{s}^{-1}$ ) for the Malin shelf. (a) The baroclinic energy flux and the transport  
 549 driven by: (a) the time-mean Eulerian transport, (b) the time-mean bolus contribution from the  
 550 correlation of velocity and layer thickness, (c) the time-mean shear contribution evaluated from  
 551 the departures from the time-mean isopycnal depth, and (d) the Stokes' transport from the sum  
 552 of the bolus and shear contributions. Lines as in Fig. 8.

543 lin shelf, the Eulerian transport is much larger than the Stokes' transport, but does not  
 544 have a vertical structure that opposes the Stokes' transport (Fig. 9a); the Stokes' trans-  
 545 port signals are relatively weak and it is difficult to identify the extent of any compen-  
 546 sation.

#### 553 4.4.3 European Celtic Sea shelf

554 In the Celtic Sea, there is a more complex response with the internal tide not propa-  
 555 gating onto the shelf, but rather directed parallel to the shelf break (Fig. 10a). This  
 556 tidal propagation is a result of localisation by small scale topography at the shelf break  
 557 [Vlasenko *et al.*, 2014]. The bolus and shear components are consistent with the expected  
 558 theoretical structure, in the same and opposing direction as the internal tide propaga-  
 559 tion respectively, and there is a near cancellation in the vertical (Fig. 10b,c). As a re-  
 560 sult the layered Stokes' transport is also directed parallel to the shelf break, leading to



568 **Figure 10.** Baroclinic energy flux ( $\text{W m}^{-1}$ ), Stokes' transport, and contributions per unit  
 569 horizontal length ( $\text{m}^2\text{s}^{-1}$ ) for the Celtic Sea. (a) The baroclinic energy flux and the transport  
 570 driven by: (a) the time-mean Eulerian transport, (b) the time-mean bolus contribution from the  
 571 correlation of velocity and layer thickness, (c) the time-mean shear contribution evaluated from  
 572 the departures from the time-mean isopycnal depth, and (d) the Stokes' transport from the sum  
 573 of the bolus and shear contributions. Lines as in Fig. 8.

561 only limited open ocean - shelf sea exchange at this site. However, on larger scales, it  
 562 would still be expected that the internal tide eventually propagates onto the shelf [*In-*  
 563 *all et al.*, 2011] and with an accompanying Stokes' transport. In the Celtic sea, the Eu-  
 564 lerian transport is directed along the slope and shows a two-layer flow (Fig. 10a). This  
 565 transport structure again makes it difficult to reveal any potential cancellation, since the  
 566 Eulerian flow is in the same direction as the Stokes' transport for the bottom and mid-  
 567 dle layers and is weaker than the Stokes' transport in the middle layer.

#### 574 4.5 Summary

575 The internal tide provides a Stokes' transport that can cross the shelf break. Rep-  
 576 resenting the ocean and shelf region by three density layers, the Stokes' transport from

**Table 2.** Table of Stokes' transports in the direction of the baroclinic energy flux calculated from the moorings for each layer and the depth total. The 99 % confidence intervals are given in brackets and have been calculated as described in Section 4.2.

| Parameter                                 | Surface                      | Middle                          | Bottom                        | Total                         |
|-------------------------------------------|------------------------------|---------------------------------|-------------------------------|-------------------------------|
| <b>New Zealand (NZ)</b>                   |                              |                                 |                               |                               |
| Layer Thickness (m)                       | <b>25.6</b> (25.3 – 25.9)    | <b>34.9</b> (34.7 – 35.2)       | <b>12.4</b> (12.1 – 12.7)     | <b>72.9</b> (72.5 – 73.3)     |
| Volume Flux ( $\text{m}^2\text{s}^{-1}$ ) | <b>0.26</b> (0.22 – 0.29)    | <b>-0.73</b> (-0.76 – -0.70)    | <b>0.47</b> (0.42 – 0.51)     | <b>-0.01</b> (-0.07 – 0.06)   |
| Velocity ( $\text{cm s}^{-1}$ )           | <b>1.00</b> (0.85 – 1.15)    | <b>-2.10</b> (-2.19 – -2.01)    | <b>3.76</b> (3.41 – 4.13)     | <b>-0.02</b> (-0.11 – 0.08)   |
| <b>Malin Shelf (SG)</b>                   |                              |                                 |                               |                               |
| Layer Thickness (m)                       | <b>24.5</b> (24.4 – 24.5)    | <b>12.4</b> (12.3 – 12.4)       | <b>65.2</b> (65.1 – 65.2)     | <b>102.0</b> (101.9 – 102.1)  |
| Volume Flux ( $\text{m}^2\text{s}^{-1}$ ) | <b>0.020</b> (0.007 – 0.031) | <b>-0.035</b> (-0.045 – -0.024) | <b>0.025</b> (-0.004 – 0.055) | <b>0.010</b> (-0.022 – 0.046) |
| Velocity ( $\text{cm s}^{-1}$ )           | <b>0.080</b> (0.026 – 0.13)  | <b>-0.28</b> (-0.37 – -0.20)    | <b>0.038</b> (0.006 – 0.085)  | <b>0.010</b> (-0.021 – 0.045) |
| <b>Celtic Sea (ST4)</b>                   |                              |                                 |                               |                               |
| Layer Thickness (m)                       | <b>16.3</b> (16.2 – 16.4)    | <b>27.3</b> (27.2 – 27.4)       | <b>92.4</b> (92.3 – 92.4)     | <b>136.0</b> (135.9 – 136.1)  |
| Volume Flux ( $\text{m}^2\text{s}^{-1}$ ) | <b>0.33</b> (0.31 – 0.34)    | <b>-0.43</b> (-0.44 – -0.42)    | <b>0.15</b> (0.09 – 0.22)     | <b>0.05</b> (-0.01 – 0.12)    |
| Velocity ( $\text{cm s}^{-1}$ )           | <b>2.0</b> (1.9 – 2.1)       | <b>-1.6</b> (-1.6 – -1.5)       | <b>0.17</b> (0.09 – 0.23)     | <b>0.039</b> (-0.007 – 0.088) |

577 an internal tide consists of an onshore bolus contribution in the light upper layer and  
 578 the dense bottom layer at the shelf break, which is offset by a return volume transport  
 579 by a velocity shear contribution in the pycnocline. The Stokes' transport integrates to  
 580 zero over the whole fluid depth. On the New Zealand and Celtic Sea Shelves, the Eu-  
 581 lerian transport does not cancel the Stokes' transport and on the Malin Shelf the cross-  
 582 shelf signals are too small to infer the extent of any cancellation.

## 583 **5 Tracer transport from the internal tide directed across the shelf break**

584 The internal tide provides a Stokes' transport within a density layer, which may  
 585 then provide a tracer transport across the shelf break. In order to understand this con-  
 586 nection, consider the exchange of a tracer between the stratified ocean and the well-mixed  
 587 shelf seas within three different density layers. If we only consider the tracer exchange  
 588 across the shelf break in the  $x$ -direction and assume that the only process providing an  
 589 exchange is the Stokes' velocity,  $u_S$ , then the tendency of the tracer  $c$  is given by

$$\frac{\partial c}{\partial t} = -\frac{\partial}{\partial x}(F_c) + Q, \quad (9)$$

590 where  $Q$  is a tracer source. The tracer transport,  $F_c$ , per unit horizontal length is given  
 591 by the Stokes' velocity,  $u_S$ , acting on the tracer concentration,  $c$ , which is integrated over  
 592 the full depth,

$$F_c = \int_{-D}^0 u_S c \, dz, \quad (10)$$

593 where  $D$  is the depth of the water column. The tracer transport can be simply written  
 594 as a summation over 3 density layers, such that

$$F_c = \sum_{i=1}^3 u_{S,i} c_i h_i, \quad (11)$$

595 where each layer has a thickness,  $h_i$ , and tracer concentration,  $c_i$ , and  $i$  is a layer counter  
 596 from 1 to 3. At the same time, the Stokes' volume transport is expected to be zero when  
 597 integrated over the full depth [*Henderson, 2016*] consistent with our observations,

$$\sum_{i=1}^3 u_{S,i} h_i = 0. \quad (12)$$

598 The tracer concentrations transported onshore in the top and bottom layers are  
 599 the open ocean tracer values,  $c_1$  and  $c_3$ . The onshore tracer transport is then given by

$$u_{S,1} h_1 c_1 + u_{S,3} h_3 c_3. \quad (13)$$

600 If there is no tracer source in the shelf waters and there is vertical mixing making the  
 601 tracer concentration the same in each layer, then the tracer in the middle layer,  $c_2$ , that  
 602 is returned off shore is simply given by the transport-weighted values,  $c_{mix}$ , given by

$$c_{mix} = \frac{u_{S,1} h_1 c_1 + u_{S,3} h_3 c_3}{u_{S,1} h_1 + u_{S,3} h_3}. \quad (14)$$

603 If there is a tracer source on the shelf that makes the tracer concentration in the mid-  
 604 dle layer,  $c_2$ , greater than the transport-weighted tracer values brought onto the shelf,  
 605  $c_{mix}$ , then there is a systematic tracer transport from the shelf to the open ocean.

606 Conversely, if there is a tracer sink on the shelf that makes the tracer concentra-  
 607 tion in the middle layer,  $c_2$ , less than the transport-weighted tracer values brought onto  
 608 the shelf,  $c_{mix}$ , then there is a systematic tracer transport from the open ocean to the  
 609 shelf.

610 Following this generalised example, next consider the transport of heat, salt and  
 611 nitrate for the New Zealand mooring, where there is a strong Stokes' transport cross-  
 612 ing the shelf.

## 613 5.1 Observed tracer transport for the New Zealand shelf

614 The tracer transport for each layer is diagnosed at the New Zealand mooring using  
 615 a product of the mooring derived Stokes' transport and the tracer, averaged in density  
 616 space, for each layer. The values for salinity and nitrate are taken from a nearby CTD  
 617 cast. The salinity is taken from the high vertical resolution CTD data and the nitrate  
 618 is taken from 7 discrete bottle samples. These samples are distributed through the wa-  
 619 ter column with 4 in the surface layer (2, 20, 30 and 40 m depth), 2 in the middle layer  
 620 (60 and 80 m depth), and 1 in the bottom layer (100 m depth). The single nitrate sam-  
 621 ple in the bottom layer is likely to be representative of the entire layer as the high res-  
 622 olution CTD data reveals a well mixed bottom layer where the salinity in the bottom  
 623 layer varies by only 0.02 compared to 0.23 for the full profile. These tracer values are  
 624 then averaged in density ranges that match the density ranges used for the volume trans-  
 625 port to give a single value for each layer, which is then used to calculate the tracer trans-  
 626 port.

### 633 5.1.1 Heat and salt transport

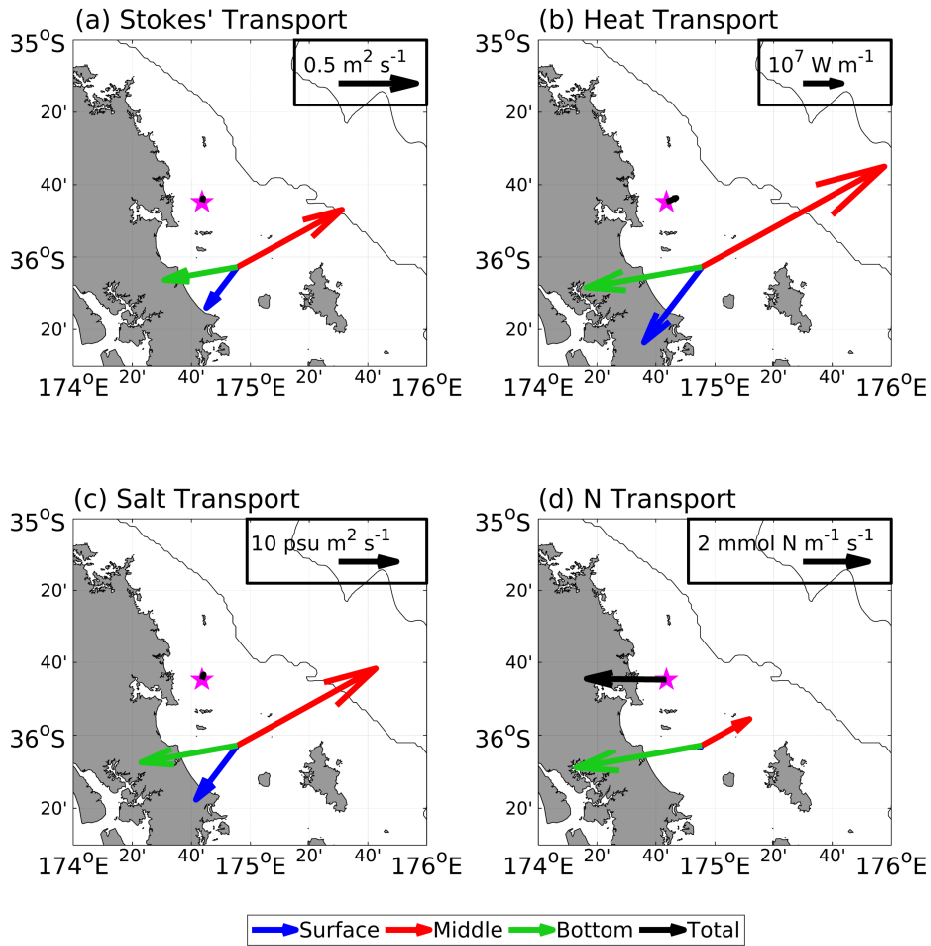
634 The vertical structure of the Stokes' transport dictates the direction of the asso-  
 635 ciated property transport, although their magnitudes for each layer are set by the prop-  
 636 erty value. There is an on shelf heat transport in the surface and bottom layers, and an  
 637 off shelf heat transport in the middle layer (Fig. 11a,b). There is not a significant depth-  
 638 integrated heat transport directed on shelf. There is a similar response for the salt flux,  
 639 an on shelf salt transport in the surface and bottom layers, and an off-shelf salt trans-  
 640 port in the middle layer (Fig. 11c). This result is equivalent to the case where there is  
 641 no source or sink of tracer on the shelf leading to the tracer returned in the middle layer  
 642 being equivalent to a linear mixture of the tracer transported in the surface and bottom  
 643 layers (as given by  $c_{mix}$  in Eqn. 14).

### 644 5.1.2 Nitrate transport

645 Nitrate has a vertical structure that differs from the vertical structure of temper-  
 646 ature and density due to the biological utilisation of nitrate in the euphotic zone and re-  
 647 generation of biological fallout at depth. The nitrate transport becomes very small in  
 648 the surface layer due to its very low nitrate concentration and the nitrate transport is  
 649 weakly off shelf in the middle layer (Fig. 11d). The nitrate transport is instead strongly  
 650 on shelf in the bottom layer due to the high concentration of nitrate from the regener-  
 651 ation of biological fallout and high concentrations at depth in the adjacent open ocean.  
 652 This overall structure of the Stokes' transport of nitrate over each layer leads to an over-  
 653 all depth-integrated on-shelf nitrate transport (Fig. 11d, black arrow), which acts to sus-  
 654 tain enhanced productivity on the shelf.

655 This net transport of nitrate can be understood by comparing the concentration  
 656 of nitrate in the off-shelf transported middle layer to the concentration expected for a  
 657 conserved tracer (Eqn. 14). Using the volume transport and nitrate concentrations in  
 658 the surface and bottom layers at the mooring gives an expected nitrate concentration  
 659 in the middle layer of  $c_{mix} = 5.42 \text{ mmol N m}^{-3}$ . This expected concentration is larger  
 660 than the observed middle layer nitrate concentration at the mooring of  $c_2 = 2.16 \text{ mmol}$   
 661  $\text{N m}^{-3}$ . The deficit of nitrate in the middle layer implies a sink on the shelf, likely driven  
 662 by biological consumption, and leads to an imbalance between the on-shelf and off-shelf  
 663 transports driving a net transport.

664 In the bottom layer, the on-shelf transport at the mooring is  $2.9 \text{ mmol m}^{-1} \text{ s}^{-1}$   
 665 which, assuming that the transport converges over the distance between the mooring and  
 666 the coast of 17 km, gives a nitrate supply and a convergence of bottom-layer nitrate trans-  
 667 port of  $1.7 \times 10^{-7} \text{ mol N m}^{-2} \text{ s}^{-1}$ . In comparison, *Sharples et al.* [2001] conducted a tur-



627 **Figure 11.** Tracer transport provided by the Stokes' volume transport calculated at the  
 628 New Zealand mooring using a combination of the mooring data and an adjacent CTD profile  
 629 with nitrate samples taken: (a) volume transport ( $\text{m}^2\text{s}^{-1}$ ), (b) heat transport ( $\text{W m}^{-1}$ ), (c)  
 630 salt transport ( $\text{psu m}^2 \text{s}^{-1}$ ), and (d) nitrate transport ( $\text{mmol N m}^{-1}\text{s}^{-1}$ ). The tracer transports are  
 631 calculated using the same layers as applied for the Stokes' volume transport and for a full depth  
 632 integral.

668 bulence study of the vertical supply of nitrate at the same time and in the same loca-  
 669 tion as the mooring, and calculated a vertical flux of nitrate into the photic zone of  $1.4 \times 10^{-7}$   
 670  $\text{mol N m}^{-2} \text{s}^{-1}$ . Hence, these two independent estimates of nitrate fluxes diagnosed ei-  
 671 ther from the moorings or from turbulence measurements are consistent with each other,  
 672 and support the view that the internal tide generates a Stokes' transport driving a hor-  
 673 izontal nitrate flux onto the shelf that sustains the vertical nitrate flux to the photic zone  
 674 associated with the turbulent mixing from the breaking of the internal tide.

## 675 6 Conclusions

676 There is a long standing problem of how tracers are transported across the con-  
 677 tinental slope. The internal tide usually propagates across the continental slope from the  
 678 open ocean to the shelf seas. There is a Stokes' transport associated with the internal  
 679 tide, which is made up of the sum of a bolus contribution and a shear contribution. This  
 680 Stokes' transport may be non-zero within an individual density layer, even though its  
 681 depth integral vanishes.

682 The propagation of the internal tide across the top of the continental slope auto-  
 683 matically leads to onshore bottom velocities coinciding with a thicker bottom layer be-  
 684 tween the thermocline and sea floor, as well as offshore upper velocities and a thinner  
 685 upper layer between the sea surface and the thermocline. There is a resulting onshore  
 686 Stokes' transport from the bolus contribution near the surface and the sea floor, which  
 687 is returned offshore in the pycnocline via the shear contribution to the Stokes' transport.  
 688 This vertical structure is consistent with the theoretical drift experienced by neutrally-  
 689 buoyant tracers and is the same in the onshore directed layers for depth-regulating phy-  
 690 toplankton [Franks *et al.*, 2019].

691 Previous theoretical work for an inviscid ocean has implied near complete cancel-  
 692 lation between the Stokes' transport and the Eulerian transport at all depths [Wunsch,  
 693 1971; Wagner and Young, 2015]. Partial cancellation was also revealed in a lake study  
 694 [Henderson, 2016]. The extent to which the assumptions underlying this previous work  
 695 apply in shelf sea observations is unclear, particularly as diapycnal mixing occurs over  
 696 the shelf allowing fluid to exchange between density layers. In the mooring data on the  
 697 New Zealand shelf, the Eulerian transports are generally directed along bathymetric con-  
 698 tours, and their cross-bathymetric components are weaker than the Stokes' transport and  
 699 do not cancel the Stokes' transport. In the remaining two moorings, any cancellation is  
 700 hard to identify as the cross-shelf components of the Eulerian transports are of a sim-  
 701 ilar magnitude to the Stokes' transport. There are a range of potential explanations for  
 702 the lack of cancellation between the Stokes' transport and Eulerian-mean transport in  
 703 the observations: spatial variability in the internal tide leading to return flow being fo-  
 704 cused in a regions of weak internal tides; temporal variability allowing the Stokes' trans-  
 705 port to drive volume fluxes until a new dynamical balance is reached between the Eu-  
 706 lerian flow and the stratification; eddy exchange at the shelf break "resetting" the strat-  
 707 ification on the shelf; or enhanced turbulence and mixing on the shelf allowing diapy-  
 708 cnal exchange between density layers. The explanation, or combination of explanations,  
 709 responsible for the lack of cancellation is unclear from these observations and requires  
 710 further research.

711 The importance of the Stokes' transport varies with the strength and orientation  
 712 of the baroclinic energy flux. For 3 different moorings, there are different regimes: a large  
 713 onshore baroclinic energy flux directed onshore in the New Zealand shelf, a weak onshore  
 714 baroclinic energy flux directed onshore in the Malin shelf and a baroclinic energy flux  
 715 directed along bathymetric contours in a region of complex topography in the Celtic shelf.

716 Now consider the different tracer sources and sinks acting over the shelf in terms  
 717 of the biogeochemistry, which might alter the tracer concentrations and lead to the Stokes'  
 718 transport providing an offshore or onshore tracer transport.

719 There is a strong signal of enhanced biological production on the shelf, forming both  
 720 particulate and dissolved organic nutrients. The dissolved organic nutrients are expected  
 721 to be transported offshore in the middle layer via the shear contribution to the Stokes'  
 722 transport. The biological productivity has to be sustained by a supply of inorganic nu-  
 723 trients, from river input, resuspension from sediments, atmospheric deposition or exchange  
 724 with the open ocean. If the shelf sources dominate, then inorganic nutrients will be trans-  
 725 ported offshore in the middle layer by the Stokes' transport. If the shelf sources are in-  
 726 sufficient to sustain the biological production, which is often the case [*Liu et al.*, 2010],  
 727 then the onshore nutrient transport in the surface and bottom layers are needed. As the  
 728 nutrient concentrations are low in surface waters, this onshore nutrient transport is pro-  
 729 vided by the bolus transport contribution to the Stokes' transport acting in the nutrient-  
 730 rich bottom layer.

731 If there are shelf inputs of trace metals, such as iron, from the sediments or river-  
 732 ine inputs, then there will be an off shelf transport of trace metals in the middle layer  
 733 via the shear contribution to the Stokes' transport. If the typical Stokes' velocities within  
 734 the pycnocline are  $0.5 \text{ cm s}^{-1}$ , then the off shelf tracer plume will extend for 500 km based  
 735 on an advective timescale of a 100 days during summer (when the surface mixed layer  
 736 in the open ocean is sufficiently shallow to allow this signal to be visible).

737 Previously, other physical processes driving exchange across the shelf break have  
 738 been identified as being important for the European Shelf, such as surface and bottom  
 739 Ekman transport. *Huthnance et al.* [2009] revealed Ekman transfers with volume trans-  
 740 ports at the slope current ( $0.5$  to  $0.8 \text{ m}^2 \text{ s}^{-1}$ ) that are larger than the Stokes' transports  
 741 calculated here ( $0.019$  to  $0.43 \text{ m}^2 \text{ s}^{-1}$ ). However the Ekman circulations are directed on  
 742 shelf near the surface and off shelf at depth for the European shelf. In the bottom layer,  
 743 this Ekman-driven circulation is opposite to the internal-tide driven Stokes' transport  
 744 indicating the potentially-important contribution by Stokes' transport in the supply of  
 745 nutrients.

746 For the New Zealand shelf, the estimate of the vertical supply of nitrate by tur-  
 747 bulent mixing [*Sharples et al.*, 2001] is of the similar magnitude to our estimate of how  
 748 the internal tide drives a Stokes' transport providing a horizontal supply of nitrate. Hence  
 749 there may be a balance between the baroclinic tide providing a horizontal onshore trans-  
 750 port of nitrate and the breaking of the internal tide providing a vertical nitrate supply.

751 In summary, the Stokes' transport for a density layer may provide a systematic trans-  
 752 port of tracers across the shelf break. Whether this tracer transport is directed off shelf  
 753 or on shelf depends on whether there is a tracer source or sink, respectively, on the shelf.  
 754 This tracer transport can be an important source of nutrients to the highly productive  
 755 shelf seas.

## 756 Acknowledgments

757 This work was supported by the UK NERC Fluxes Across Sloping Topography of the  
 758 North East Atlantic (FASTNet) programme (NE/I030216/1). The NZ mooring was part  
 759 of the Nearshore-Offshore Exchange Programme, supported by the New Zealand Foun-  
 760 dation for Research in Science and Technology. We are grateful to anonymous referees  
 761 for detailed advice and constructive feedback which have much improved this manuscript.  
 762 We are also grateful to advice and feedback from Andrew Stewart, Mark Inall and John  
 763 Huthnance, and to Juliane Wihsgott for processing the temperature data on the Malin  
 764 Shelf. The data sets analysed here are available from the British Oceanographic Data  
 765 Centre ([www.bodc.ac.uk](http://www.bodc.ac.uk)).

## References

766

767

768

769

770

771

772

773

774

775

776

777

778

779

780

781

782

783

784

785

786

787

788

789

790

791

792

793

794

795

796

797

798

799

800

801

802

803

804

805

806

807

808

809

810

811

812

813

814

815

816

817

818

- Brink, K. (1988), Deep-sea forcing and exchange processes, in *Chap 6 In: The Sea, The Global Coastal Ocean: Processes and Methods*, vol. 10, edited by K. Brink and A. Robinson, pp. 151–167, John Wiley & Sons, New York.
- Brink, K. (2016), Cross-shelf exchange, *Annual Review of Marine Science*, 8, 59 – 78.
- Franks, P. J. S., J. C. Garwood, M. Ouimet, J. Cortes, R. C. Musgrave, and A. J. Lucas (2019), Stokes drift of plankton in linear internal waves: Crossshore transport of neutrally buoyant and depthkeeping organisms, *Limnology and Oceanography*, 65, 1286–1296.
- Green, J. M., J. H. Simpson, S. Legg, and M. R. Palmer (2008), Internal waves, baroclinic energy fluxes and mixing at the European shelf edge, *Continental Shelf Research*, 28, 937–950.
- Hall, R. A., J. M. Huthnance, and R. G. Williams (2013), Internal wave reflection on shelf slopes with depth-varying stratification, *Journal of Physical Oceanography*, 43, 248 – 258.
- Henderson, S. M. (2016), Upslope internal-wave stokes drift, and compensating downslope eulerian mean currents, observed above a lakebed, *Journal of Physical Oceanography*, 46, 1947 – 1961.
- Hill, A. E. (1995), Leakage of barotropic slope currents onto the continental shelf, *Journal of Physical Oceanography*, 14, 1617 – 1621.
- Hopkins, J., J. Sharples, and J. Huthnance (2012), On-shelf transport of slope water lenses within the seasonal pycnocline, *Geophysical Research Letters*, 39, L08,604.
- Hopkins, J. E., G. R. Stephenson Jr., J. A. M. Green, M. E. Inall, and M. R. Palmer (2014), Storms modify baroclinic energy fluxes in a seasonally stratified shelf sea: Inertial-tidal interaction, *Journal of Geophysical Research Oceans*, 119, 6863 – 6883.
- Huthnance, J., J. Holt, and S. Wakelin (2009), Deep ocean exchange with west-European shelf seas, *Ocean Sciences*, 5, 621 – 634.
- Huthnance, J. M. (1984), Slope Currents and JEBAR, *Journal of Physical Oceanography*, 14, 795 – 810.
- Inall, M., G. I. Shapiro, and T. J. Sherwin (2001), Mass transport by non-linear internal waves on the malin shelf, *Continental Shelf Research*, 21, 1449 – 1472.
- Inall, M., D. Aleynik, T. Boyd, M. Palmer, and J. Sharples (2011), Internal tide coherence and decay over a wide shelf sea, *Geophys. Res. Letters*, 38, L23,607.
- Kelly, S. M., and J. D. Nash (2010), Internaltide generation and destruction by shoaling internal tides, *Geophysical Research Letters*, 37, L23,611.
- Klink, J. (1999), Dynmodes.m - ocean dynamic vertical modes. Woods Hole Science Center - SEA-MAT—Matlab tools for oceanographic Analysis.
- Legg, S., and A. Adcroft (2003), Internal wave breaking at concave and convex continental slopes, *Journal of Physical Oceanography*, 33, 2224–2246.
- Lentz, S. J. (2003), A climatology of salty intrusions over the continental shelf from Georges Bank to Cape Hatteras, *Journal of Geophysical Research Oceans*, 108(C10), doi:10.1029/2003JC001859, 3326.
- LinkQuest Inc. (2007), Flowquest 75/150/300/600/1000/2000 acoustic current profiler user guide.
- Liu, K. K., L. Atkinson, R. A. Quinones, and L. Talaue-McManus (2010), Biogeochemistry of continental margins in a global context, in *Carbon and Nutrient Fluxes in Continental Margins: A Global Synthesis*, edited by K. K. Liu, L. Atkinson, R. A. Quinones, and L. Talaue-McManus, pp. 3 – 24, Berlin Heidelberg: Springer-Verlag.
- MacCready, P. (2011), Calculating estuarine exchange flow using isohaline coordinates, *Journal of Physical Oceanography*, 41, 1116 – 1124.

- 819 MacDonald, D. G. (2006), Estimating an estuarine mixing and exchange ratio from  
820 boundary data with application to mt. hope bay (massachusetts/rhode island),  
821 *Estuarine, Coastal, and Shelf Science*, *70*, 326 – 332.
- 822 MacKinnon, J. A., and M. C. Gregg (2003), Shear and baroclinic energy flux on the  
823 summer New England Shelf, *Journal of Physical Oceanography*, *33*, 1462 – 1475.
- 824 Marshall, D. (1997), Subduction of water masses in an eddying ocean, *Journal of*  
825 *Marine Research*, *55*, 201 – 222.
- 826 McDougall, T. J., and P. C. McIntosh (2001), The temporal-residual-mean velocity.  
827 part ii: Isopycnal interpretation and the tracer and momentum equations, *Journal*  
828 *of Physical Oceanography*, *31*, 1222 – 1246.
- 829 Nash, J., M. Alford, and E. Kunze (2005), Estimating internal wave energy fluxes in  
830 the ocean, *JAOT*, *22*, 1551 – 1570.
- 831 Nash, J., E. Shroyer, S. Kelly, M. Inall, M. Levine, N. Jones, and R. Musgrave  
832 (2012), Are any coastal internal tides predictable?, *Oceanography*, *25*, 80 – 95.
- 833 Ou, H. W., and L. Maas (1986), Tidal-induced buoyancy flux and mean transverse  
834 circulation, *Continental Shelf Research*, *5*, 611 – 628.
- 835 Painter, S. C., S. E. Hartman, C. Kivimae, L. A. Salt, N. M. Clargo, Y. Bozec, C. J.  
836 Daniels, S. C. Jones, V. S. Hemsley, L. R. Munns, and S. R. Allen (2016), Carbon  
837 exchange between a shelf sea and the ocean: The hebrides shelf, west of scotland,  
838 *Journal of Geophysical Research: Oceans*, *121*, 4522 – 4544.
- 839 Rhines, P. B. (1982), Basic dynamics of the large-scale geostrophic circulation, *Sum-*  
840 *mer Study Program in Geophysical Fluid Dynamics, Woods Hole Oceanographic*  
841 *Institution*, pp. 1–45.
- 842 Sharples, J., C. M. Moore, and E. R. Abraham (2001), Internal tide dissipation,  
843 mixing, and vertical nitrate flux at the shelf edge of NE New Zealand, *Journal of*  
844 *Geophysical Research*, *106*, 14,069 – 14,081.
- 845 Short, J., T. Doyle, J. Hopkins, J. Wihsgott, E. Dumont, and C. Griffiths (2013),  
846 Moorings, in *RRS James Cook Cruise JC88, Glasgow to Southampton, FASTNet*  
847 *Cruise to the Malin Shelf Edge*, edited by M. Inall, no. XX in Internal Report,  
848 chap. 13, pp. 102 – 130, Scottish Association for Marine Science.
- 849 Simpson, J. H., and R. R. McCandless (2012), "The Ekman Drain": a conduit to the  
850 deep ocean for shelf material, *Ocean Dynamics*, *63*, 1063 – 1072.
- 851 Stephenson Jr., G. R., J. E. Hopkins, J. A. M. Green, M. E. Inall, and M. R. Palmer  
852 (2015), Baroclinic energy flux at the continental shelf edge modified by wind-  
853 mixing, *Geophysical Research Letters*, *42*, 1826 – 1833.
- 854 Stewart, A. L., and A. F. Thompson (2015), Eddy-mediated transport of warm  
855 circumpolar deep water across the antarctic shelf break, *Geophysical Research*  
856 *Letters*, *42*, 432 – 440.
- 857 Stewart, A. L., A. Klocker, and D. Menemenlis (2019), Acceleration and overturn-  
858 ing of the antarctic slope current by winds, eddies, and tides, *Journal of Physical*  
859 *Oceanography*, *49*, 2043 – 2074.
- 860 Thomas, J., O. Buhler, and K. S. Smith (2018), Wave-induced mean flows in rotat-  
861 ing shallow water with uniform potential vorticity, *Journal of Fluid Mechanics*,  
862 *839*, 408 – 429.
- 863 Thorpe, S. A. (1968), On the shape of progressive internal waves, *Philosophical*  
864 *transactions of the Royal Society of London A*, *263*, 563 – 614.
- 865 Vlasenko, V., N. Stashchuk, M. E. Inall, and J. E. Hopkins (2014), Tidal energy  
866 conversion in a global hotspot: On the 3-D dynamics of baroclinic tides at  
867 the Celtic Sea shelf break, *Journal of Geophysical Research Oceans*, *119*, doi:  
868 10.1002/2013JC009708.
- 869 Wagner, G. L., and W. R. Young (2015), Available potential vorticity and wave-  
870 averaged quasi-geostrophic flow, *Journal of Fluid Mechanics*, *785*, 401 – 424.
- 871 Weber, J. E. H., and K. H. C. G. Brostrom (2014), Stokes drift in internal equato-  
872 rial kelvin waves: Continuous stratification versus two-layer models, *Journal of*

873 *Physical Oceanography*, 44, 591 – 599.

874 Wunsch, C. (1971), Note on some reynolds stress effects of internal waves on slopes,  
875 *Deep-Sea Research*, 18, 583–591.

876 Zhang, S., M. H. Alford, and J. B. Mickett (2015), Characteristics, generation and  
877 mass transport of nonlinear internal waves on the washington continental shelf,  
878 *Journal of Geophysical Research: Oceans*, 120, 741 – 758.